Published in Boreas 47 (2018), 544–564

Chronostratigraphy and spatial distribution of magnetic sediments in the Chukchi and Beaufort seas since the last deglaciation

CHARLES-EDOUARD DESCHAMPS, GUILLAUME ST-ONGE, JEAN-CARLOS MONTERO-SERRANO AND LEONID POLYAK

Deschamps, C.-E., St-Onge, G., Montero-Serrano, J.-C. & Polyak, L.: Chronostratigraphy and spatial distribution of magnetic sediments in the Chukchi and Beaufort seas since the last deglaciation.

Palaeomagnetic investigation of three sediment cores from the Chukchi and Beaufort Sea margins was performed for better constraining the regional chronostratigraphy and for gaining insights into sediment magnetic properties at the North American Arctic margin during the Holocene and the preceding deglaciation. Palaeomagnetic analyses reveal that sediments under study are characterized by low-coercivity ferrimagnetic minerals (magnetite), mostly in the pseudo-single domain grain-size range, and by a strong, stable, well-defined remanent magnetization (MAD <5°). Age models for these sediment cores were constrained by comparing their palaeomagnetic secular variations (inclination, declination, and relative palaeointensity) with previously published and independently dated sedimentary marine records from the study area. The magnetostratigraphic age models were verified by AMS radiocarbon dating tie points in the AMD cores and by tephrochronology and ^{210}Pb-based sedimentation rate estimate for 01JPC. The analyzed cores 01JPC, 03PC and 02PC span ~6000, 10 500 and 13 500 cal. a BP, respectively. The estimated sedimentation rates were stable and relatively high since the deglaciation in cores 01JPC (60 cm ka^{-1}) and 03PC (40-70 cm ka^{-1}). Core 02PC shows much lower Holocene sedimentation rates with a strong decrease after the deglaciation from ~60 to 10-20 cm ka^{-1}. Overall, this

study illustrates the usefulness of palaeomagnetism to improve the dating of Late Quaternary sedimentary records in the Arctic Ocean.

Deschamps Charles-Edouard (corresponding author: deschampscharlesedouard@gmail.com), Guillaume St-Onge and Jean-Carlos Montero-Serrano, Institut des sciences de la mer de Rimouski, Canada Research Chair in Marine Geology, Université du Québec à Rimouski & GEOTOP, 310 allée des Ursulines, Rimouski, Québec, G5L 3A; Canada. Leonid Polyak, Byrd Polar and Climate Research Center, Ohio State University, Columbus, OH 43210, USA

Radiocarbon dating is the most widespread method used to determine the age of fossils or organic matter deposited in marine sediment cores during the last ~40-50 ka. However, the scarcity and poor preservation of calcareous tests and a high content of redeposited terrestrial organic matter in the Arctic Ocean complicates the dating of sediments (Ledu *et al.* 2008; McKay *et al.* 2008; Barletta *et al.* 2010). Moreover, radiocarbon dating in the Arctic is complicated by an often poorly constrained radiocarbon reservoir age (Hanslik *et al.* 2010). Consequently, palaeoceanographic reconstructions in this climatically sensitive region are hampered by a lack of robust chronologies. One tool that has a potential to circumvent these difficulties is palaeomagnetism, which can be used to reconstruct centennial/millennial-scale variations in the Earth's magnetic field and to identify regional chronostratigraphic markers by observing synchronous changes such as inclination, declination, or intensity of the magnetic field (Barletta *et al.* 2008, 2010; Darby *et al.* 2012; Lund *et al.* 2016). As a result, palaeomagnetism helps to establish the age control in chronostratigraphically challenging environments (St-Onge *et al.* 2007; Stoner & St-Onge 2007).

A few studies have used magnetostratigraphy as a regional dating tool for Holocene sediments on the western Arctic continental margins in the absence of datable material or to independently support and improve chronostratigraphy based on radiocarbon dating (Barletta *et al.* 2008, 2010; Lisé-Pronovost *et al.* 2009; Darby *et al.* 2012). These studies have compared the identified chronostratigraphic markers with Holocene palaeomagnetic curves, such as for western North American volcanic rocks (PSVL; Hagstrum & Champion 2002) or Grandfather Lake sediments in Alaska (GFL; Geiss & Banerjee 2003), and also with global geomagnetic field models (CALS7k.2) based on spherical harmonic analysis (Korte & Constable 2005). However, most of the palaeomagnetic records generated in the Beaufort Sea fall short of recovering the entire Holocene and the deglacial sediments (Barletta *et al.* 2008, 2010; Lisé-Pronovost *et al.* 2009). This lack of data on palaeomagnetic secular variation in the lower Holocene and deglaciation is mainly due to the use of cores recovered by relatively short piston coring at sites with high sedimentation rates (>100 cm ka^{-1}; Barletta *et al.* 2008; Darby *et al.* 2009). In stratigraphically longer records studied at the Chukchi margin, the deglacial sediments contained numerous ice-rafted debris (IRD), which makes them unsuitable for palaeomagnetic reconstructions (Barletta *et al.* 2008; Lisé-Pronovost *et al.* 2009).

In this paper, we present the full-vector palaeomagnetic records (inclination, declination, and relative palaeointensity) of three piston cores from the Alaska-Chukchi and Beaufort margins, as well as the magnetic properties of several sediment cores along the North American margin (Fig. 1) in order to improve the chronostratigraphy of the Holocene to deglacial sediments in the western Arctic Ocean and characterize the sedimentary processes influencing the magnetic parameters along the Beaufort and Chukchi shelves.

Regional setting

The shallow Chukchi and Beaufort Sea margins was flooded last time during the glacial/Holocene transition (Keigwin *et al.* 2006). The Chukchi shelf circulation is controlled by an inflow of Pacific waters via the Bering Strait, the Siberian coastal current, and the Atlantic Intermediate Water affecting the northern margin (Pickart 2004; Weingartner *et al.* 2005). Modern sediment in the Chukchi Sea is believed to be mainly derived from northeastern Siberia and Bering Strait inflow (especially from the Yukon River), whereas, the Beaufort margin sediment originates primarily from the Mackenzie River basin (Viscosi-Shirley *et al.* 2003; Ortiz *et al.* 2009; Asahara *et al.* 2012). Smaller Alaskan rivers have a more local impact but may have been a more important sediment source at the early stages of the last transgression (Hill & Driscoll 2008). The ice-rafted debris (IRD) is also an important sediment component in the Chukchi and Beaufort seas (Darby 2003; Ortiz *et al.* 2009). In modern and Holocene sediments the IRD may originate from multiple sources including local and distant provenance, depending on circulation that controls the ice drift (Darby & Bischof 2004; Darby *et al.* 2012; Polyak *et al.* 2016).

The Canadian Beaufort Shelf occupies a broad, rectangular area (about 120 km of width and 530 km of length) bordered by the Amundsen Gulf to the east, Mackenzie Canyon to the west, the Mackenzie River delta to the south, and the deep basin of the Beaufort Sea to the north. Sedimentation on the Canadian Beaufort Shelf is mostly influenced by the Mackenzie River plume (Richerol *et al.* 2008). Although the Mackenzie River discharges less water (~420 km^3 a^{-1}; Wagner *et al.* 2011) than the Siberian rivers, the suspended sediment load from the Mackenzie River is three to four times higher than from the Siberian rivers (Matthiessen *et al.* 2000). The total sediment load delivered to the head of the delta reaches up to 128 Mt a^{-1} (Carson *et al.* 1998; O'Brien *et al.* 2006), which explains very high sedimentation rates in this area (about 30 to 320 cm ka^{-1}; Barletta *et al.* 2008, 2010; Bringué & Rochon 2012; Durantou *et al.* 2012).

During deglaciation and the early Holocene, sediment inputs to the Chukchi and Beaufort margins were presumably higher than at later times due to the rising sea level associated with meltwater and iceberg discharge from the retreating Laurentide Ice Sheet, although the age control for these sediments is not well constrained (Hill *et al.* 2007; Hill & Driscoll 2008; Scott *et al.* 2009). The deglacial/glacial IRD was derived primarily from the Laurentide provenance, such as the Canadian Arctic Archipelago, that has characteristically high content of dolomites (Phillips & Grantz 2001; Stokes *et al.* 2005; Polyak *et al.* 2007; Schell *et al.* 2008).

Material and methods

Coring sites.

Cores HLY0501-01JPC/TWC (jumbo piston core and attendant trigger weight core) and HLY0501-01MC (multicore), hereinafter collectively referred to as 01JPC, were raised from the Chukchi-Alaskan margin from the USCGC Healy as part of the 2005 Healy-Oden Trans-Arctic Expedition (HOTRAX) (Darby *et al.* 2005). Cores 1JPC/TWC were recovered in a slope canyon about 100 km north of Barrow at 1163 m water depth (Table 1, Fig. 1). The multicore 1MC was recovered nearby, but the exact water depth was not recorded.

Cores AMD0214-02PC/TWC and AMD0214-03PC/TWC (hereinafter referred to as 02PC and 03PC) were collected from the CCGS Amundsen during the 2014 ArcticNet expedition (Deschamps *et al.* 2014). These cores were recovered at the Canadian Beaufort margin, with core 03PC located in front of the Mackenzie River delta (Table 1, Fig. 1).

Magnetic properties of several cores investigated in earlier studies have been used for comparison with the data presented in this paper. These cores included HLY0501-05JPC (Barletta *et al*. 2008), HLY0501-06JPC and HLY0501-08JPC (Lisé-Pronovost *et al*. 2009) and also HLY0203-16JPC (Darby *et al.* 2012) from the Chukchi Sea, as well as cores 2004-804-650PC and 2004-804-803PC (Barletta *et al*. 2010) from the Beaufort Shelf. Cores PC1, PC2, PC3 (Schell *et al*. 2008) and 2004-804-750PC (Scott *et al.* 2009) from the Canadian Beaufort margin were used for the age model comparison. The Chukchi-Alaskan cores were hereinafter referred to 05JPC, 06JPC, 08JPC and 16JPC.

Multi Sensor Core Logger analysis and core sampling

The bulk density (obtained by gamma ray attenuation) and volumetric magnetic susceptibility (κ_{LF}) of all the sediment cores were measured using a GEOTEK Multi Sensor Core Logger (MSCL) at 1-cm intervals. Diffuse spectral reflectance data (sediment colour) were also acquired at 1-cm resolution immediately after splitting the cores using a Minolta CM-2600d handheld spectrophotometer and then converted into the L*, a*, b* colour space of the International Commission on Illumination (CIE). L* is a black-to-white scale (0 to 100), a* is a green-to-red scale (-60 to +60), and b* is a blue-to-yellow scale (-60 to +60) (St-Onge *et al.* 2007; Debret *et al.* 2011). The MSCL and diffuse spectral reflectance analyses were performed onboard for core 01JPC and at the Institut des sciences de la mer de Rimouski (ISMER, Canada) for cores 03PC and 02PC.

All cores were sampled with u-channels (u-shaped plastic liners 2×2 cm in cross-section and up to 1.5 m in length) for palaeomagnetic analyses. Cores 02PC and 03PC were also ran through a CT scanner at the Institut national de recherche scientifique – Centre eau, terre et environnement (INRS-ETE, Québec, Canada). The resulting digital X-ray images were displayed in grey scale and expressed as CT numbers, which primarily reflects changes in bulk density (St-Onge *et al.* 2007; St-Onge & Long 2009). Cores 01JPC, 02PC, and 03PC were systematically sampled at every 20 cm (except for core 02PC, where IRD intervals were additionally sub-sampled) and correspond to a total of 21, 31, and 27 samples, respectively, used for grain-size and rock magnetism analyses.

Grain-size analyses

Sediment grain-size analyses were performed on the sediment bulk fraction using a Beckman Coulter LS13320 laser diffraction grain-size analyzer, which has a detection range of 0.04–2000 μm. Samples were deflocculated by mixing about 0.5 g of wet sediment with Calgon electrolytic solution (sodium hexametaphosphate, 20 g L^{-1}) and subsequently shaking for at least 3 h using an in-house rotator. The grain-size distribution and statistical parameters (e.g. mean and sorting) were calculated using the moment methods from the GRADISTAT software (Blott & Pye 2001).

Carbon analyses

Total carbon (C_{total}) and organic carbon (C_{org}) contents for core HLY01-MC were determined on the bulk and carbonate-free fraction using a CHN Elemental Analyser (COSTECH 4010). The carbonate-free fraction was obtained by double 10% HCl treatment. Precision was better than 1% based on an internal standard (acetanilide) and replicate samples. A blank capsule was also analysed in every run to confirm the absence of contamination.

Palaeomagnetic analysis

Palaeomagnetic data were acquired at 1-cm intervals on u-channel samples using a high-resolution 2G Enterprises™ cryogenic magnetometer model 755 SRM and pulse magnetizer module (for Isothermal Remanent Magnetization, IRM, and Saturated Isothermal Remanent Magnetization, SIRM) at the Institut des sciences de la mer de Rimouski (ISMER, Canada). The natural remanent magnetization (NRM) was stepwise demagnetized and measured with 15 steps (0, 5, 10, 15, 20, 25, 30, 35, 40, 45, 50, 55, 60, 70, and 80 mT). The anhysteretic remanent magnetization (ARM) was induced in a peak alternative field of 100 mT in the presence of a weak direct current (DC) biasing field of 0.05 mT. The isothermal remanent magnetization (IRM) and saturated isothermal remanent magnetization (SIRM) were induced using the pulse magnetizer in a DC field of 0.3 and 0.95 T, respectively. ARM, IRM, and SIRM were demagnetized with the same step as the NRM. The ARM was also expressed as anhysteretic susceptibility (k_{ARM}) by normalizing the ARM with the DC bias field. The median destructive field (MDF) of the NRM (labelled as MDF_{NRM}) expresses the value of the peak AF necessary to reduce the NRM intensity to half of its initial value and was calculated using the software developed by Mazaud (2005).

In order to determine the characteristic remanent magnetization (ChRM), the magnetic declination and inclination of the ChRM (labelled ChRM D and ChRM I, respectively) was computed with nine demagnetization steps between 15 and 55 mT for cores 02PC and 03PC at 1-cm intervals using standard principal component analysis (Kirschvink 1980) which also provides the maximum angular deviation (MAD) values. The same procedure has been carried out for core 01JPC, but using 11 demagnetization steps between 10 and 60 mT. Furthermore, the ChRM declinations were corrected for rotation at section breaks and corrected for similar circular values (e.g. 0 and 360°) to derive a continuous record. MAD values lower than 5° are indicative of high-quality directional data (Stoner & St-Onge 2007). In the absence of azimuthal orientation during coring and for better comparison with previously published results, the declinations were corrected to provide an arbitrary mean declination of 0° over the time interval. Estimation of the relative palaeointensity (RPI) from sediments is obtained by normalizing the measured NRM by an appropriate magnetic parameter in order to compensate for the variable concentration of ferrimagnetic minerals (Tauxe 1993). The RPI calculated for the different cores were standardized according to their mean and standard deviation (Barletta *et al.* 2010). Changes in inclination, declination and RPI are used in this study to establish a relative stratigraphy by comparing our new records with other independently dated palaeomagnetic records from the Western Arctic.

Bulk magnetic properties

The magnetic assemblages were determined by measuring the hysteresis properties and the back-field remanence using a MicroMag 2900 alternating gradient force magnetometer (AGM) from Princeton Measurements Corporation. Both measurements were used to determine magnetic parameters such as Ms (saturation magnetization), Mrs (saturation remanence), Hc (bulk coercive force), and Hcr (remanent coercive force). The Mrs/Ms and Hcr/Hc ratios can be used as grain-size proxies (the so-called Day plot), as well as to identify the magnetic domain state when the main remanence-carrier mineral is magnetite (Day *et al.* 1977; Dunlop 2002a, b).

^{210}Pb and radiocarbon analysis

In order to support the chronostratigraphic framework derived from the palaeomagnetic data, we used three radiocarbon (^{14}C) dates of foraminiferal tests in cores 02PC and 03PC, a cryptotephra study in 01-JPC/TWC (Ponomareva *et al.* 2014), and excess ^{210}Pb age estimation for the top 15 cm sediment in 01JPC-MC. Excess ^{210}Pb measurements were made by counting the activity of the daughter isotope ^{210}Pb, ^{210}Pb ($t_{1/2}$ = 138.4 days, a = 5.30 MeV) at the GEOTOP research centre (Montréal, Canada). No foraminifera were recovered in core HLY01 while considerably high numbers of foraminifera were only found at 200, 370 and 132 cm in cores 03PC and 02PC, respectively. In order to collect sufficient amounts of foraminifera for accelerator mass spectrometry (AMS) analysis, intervals of 3 to 4 cm were sampled and sieved from cores 03PC (204-206 cm, 368-372 cm) and 02PC (131-133 cm) in both the working and archive halves (Table 2). AMS ^{14}C measurements were performed on mixed planktonic and benthic foraminifera at Beta Analytic Inc. (Miami, Florida) and LSCE (Laboratoire des Sciences du Climat et de l'Environnement, Paris, France). Radiocarbon ages were calibrated using the CALIB version 7.1 software (Stuiver & Reimer 1986–2017; http://calib.org/calib/) and the Marine13 calibration curve (Reimer *et al.* 2013). A standard oceanic reservoir age of 400 years and a regional reservoir correction (ΔR) of 400 years was applied (total: 800 years) based on the average ΔR values derived from the dates measured on five mollusc shells collected in Amundsen Gulf prior to nuclear testing (Andrews & Dunhill 2004; McNeely *et al.* 2006; Scott *et al.* 2009). The use of this ΔR value is also supported by a comparison of palaeomagnetic data for cores 2004-804-803PC and 2004-804-650PC with other well-dated Northern Hemisphere palaeomagnetic records (Barletta *et al*. 2010).

Age modelling

The non-linear relation between radiocarbon and calendar time-scales often causes single-calibrated ^{14}C ages to have very large and sometimes disparate ranges of possible calendar ages (Yeloff *et al.* 2006).

Moreover, the age–depth model constructed using a linear interpolation between the dated levels assumes that abrupt changes in accumulation rates took place exactly at the dated depths. Although this assumption is often likely to be wrong, linear interpolation frequently produces seemingly plausible age–depth models (Blaauw 2010). In this paper, the R software package BACON (Blaauw & Christen 2011) was used to produce the “best fit” linearly interpolated age models. BACON uses a Bayesian approach to estimate the best fit or weighted mean age for each depth with a 95% confidence interval that allows us to calibrate single radiocarbon ages and take into account other chronostratigraphic markers (such as cryptotephra and palaeomagnetic tie points).

Results

Stratigraphy

The correlation of the physical and magnetic parameters measured on the piston cores (PC) and their companion trigger weight cores (TWC) suggests that about 110, 10, and 5 cm of sediments were lost during piston coring at the top of cores 01JPC, 02PC, and 03PC, respectively. Therefore, a composite succession has been constructed for core 01JPC using the TWC and JPC data in order to obtain a full reconstruction of palaeomagnetic vectors (Fig. 2). Note that 1.5 m sediment are missing between section 3 and 4 of HLY01-JPC during coring operation (Darby *et al*. 2005). However this study only focuses on the first two sections of the 01JPC. Similarly, the missing sediment at the top of cores 03PC and 02PC was taken into account and all depths are hereafter expressed as corrected depths. We note that matching of piston and trigger cores is inevitably approximate due to potentially different compression/extension of sediment in individual cores.

According to the visual description, core 01JPC can be subdivided into two main lithological units (Fig. 3). Unit II (400–320 cm) consists of laminated brown to grey (Munsell colour 5Y 4/1) silty muds with dropstones typical of postglacial sediments on the Chukchi-Alaskan margin (Darby *et al.* 2006; Barletta *et al.* 2008, 2010; Lisé-Pronovost *et al.* 2009). In addition, the sediment contains numerous black speckles throughout that are likely iron sulphides (Brachfeld *et al.* 2009; Lisé-Pronovost *et al.* 2009).

A significant change in all the physical and magnetic parameters occurs at 320 cm, corresponding to the boundary with Unit I. We also observed a small decrease for the mean grain size from 6 to 4 μm (Fig. 3). Lithological units Ia and Ib mainly comprise homogenous silty mud and the only difference is related to a slight change in sediment colour: Unit Ia is grey (5Y 5/1) and Unit Ib is olive grey (5Y 5/2) (Fig. 3). This lithostratigraphic unit has been identified in the study area as Holocene marine deposit resulting from a combination of sediment drift and ice-rafted material (Darby 2003; Polyak *et al.* 2007, 2016; Darby *et al.* 2009).

Abundant cryptotephras were counted in the upper part of core 01JPC with the main peak identified at 157 cm in the composite sequence (Fig. 3). Based on geochemical composition (including major, trace and rare earth elements), both dacitic and andesitic populations of glasses have similar patterns to bulk analyses of dacitic and andesitic tephras of the Aniakchak II eruption in southern Alaska (Ponomareva *et al*. 2014; V. Ponomareva, pers. comm. 2016). Tephra layers with a similar geochemical composition have been reported from lake cores in Alaska (Kaufman *et al.* 2012), eastern Canada (Pyne-O'Donnell 2011), Greenland GRIP and NGRIP ice cores (Pearce *et al.* 2004; Coulter *et al.* 2012) and western Chukchi Sea (Pearce *et al.* 2016) and were dated to ~3.6 cal ka BP.

Based on CT-scan imaging of core 03PC, density gradually decreases throughout the core, along with the transition from laminated sediment at the base to homogenous sediment at the top, which allows us to subdivide it into three main lithological units (Fig. 3). Despite the lithological changes, the mean grain size is quite constant along core 03PC (~3 μm; Fig. 3). In Unit III (from the base to 280 cm), the sediments are characterized by laminated olive-grey (5Y 5/2) fine muds. Likewise, numerous darker (5Y 3/2) laminations occur in this unit between 380 and 520 cm. The middle part of Unit III has been dated to 7590 cal. a BP (Table 2, Fig. 3). Similar laminations have also been observed in sediment cores from the Alaskan shelf (Andrews & Dunhill 2004) and Mackenzie Trough (Schell *et al*. 2008) and interpreted as the result of increased water column stratification related to deglacial environments dated to around 11 500 cal. a BP in Schell *et al*. (2008). Between 180 and 280 cm (Unit II), the sediments are represented by a gradual lithological transition of olive-grey (5Y 4/2) laminated mud to dark-grey (5Y 4/1) faintly laminated mud. The upper part of Unit II has been dated to 5831 cal. a BP (Table 2, Fig. 3). From 0 to 180 cm (Unit I), sediments consist of homogeneous dark grey (5Y 4/1) mud to olive brown (2.5Y 4/3) mud.

02PC CT-scan imaging is quite similar to core 03PC, with a decrease in density associated with laminated sediments grading into homogeneous sediments from the base to the top of the core (Fig. 3). However, two additional major high-density intervals associated with a grain size increase (from 3 to 6 µm) can be observed between 140 and 170 cm (IRD1) and between 330 and 355 cm (IRD2, Fig. 3). For sediment core 02PC, the sediments consist of dark-grey (5Y 4/1) mud with laminations on the CT-scan imaging between 170 to 320 cm, as well as from 355 cm to the base of the core (Unit II) (Fig. 3). From 0 to 130 cm (Unit I), it consists of homogeneous olive-brown (2.5Y 4/3) to dark-grey (5Y 4/1) silt with a mean grain size ranging from 3 to 4 µm (Fig. 3). The base of Unit I have been dated 6160 cal. a BP (Table 2, Fig. 3). IRD layers 1 and 2 have also been identified in the nearby core 2004-804-750PC (Scott *et al*. 2009) and dated to 11 580 and 13 500 cal. a BP, respectively (Fig. S1). Furthermore, the white clasts in deglacial sediments from this region were previously recognised to be detrital carbonate (dolomite) transported as IRD from the Canadian Arctic Archipelago during the disintegration of the Laurentide Ice Sheet (Polyak *et al.* 2007; Scott *et al.* 2009). Similar dolomitic clasts were found in glacial/deglacial intervals in sediment cores across the entire western Arctic Ocean (Phillips & Grantz 2001; Polyak *et al.* 2009; Scott *et al.* 2009; Hillaire-Marcel *et al.* 2013).

^{210}Pb and carbon data (core 01MC)

No evidence of correlation can be identified between cores 01MC and 01TWC by means of optical properties, which could indicate missing sediment from the top of core 01TWC (Fig. S2). On the other hand, the ^{210}Pb profile for 01MC illustrates a clear exponential decrease in the top 10 cm then an increasing trend at 11 cm in the sediment (Fig. S3). The increase in unsupported ^{210}Pb at 10.5 cm can be explained by an accumulation of organic matter at this depth (shown by the C_{org} profile in Fig. S3). The minimal value in the observed supported Pb is 5.1 dpm g^{-1} (Fig. S3), consistent with the 4–5 dpm g^{-1} values reported for the Beaufort Sea (Scott *et al*. 2009; Bringué & Rochon 2012). The neperian logarithm of the excess ^{210}Pb plotted against depth in core 01MC indicates an average sedimentation rate of 65 cm ka^{-1} (Fig. S3).

Magnetic mineralogy

The pseudo S-ratio (St-Onge *et al.* 2003) in core 01JPC is close to 1, with a mean value of 0.99 for Unit I and 0.95 for Unit II sediment. The pseudo S-ratio is similar for the different lithological units for cores 03PC and 02PC, with mean values of 0.94 and 0.96 respectively. These values close to 1 indicate that saturation of the magnetic assemblage is achieved in a 0.3 T field, which is typical of low-coercivity minerals such as magnetite and/or titanomagnetite (Stoner & St-Onge 2007) (Fig. 3). Furthermore, the shape of the hysteresis curves from the three sediment cores (Fig. 4A) is also characteristic of low-coercivity ferrimagnetic minerals like magnetite (Tauxe *et al.* 1996).

The MDF_{NRM} values are continuous for lithological Unit II (mean value of 27.60 mT) and increase in Unit I, with a mean value of 38.72 mT in core HLY01 (Fig. 3). In core 03PC, the MDF_{NRM} varies throughout the core, but increases from Unit III to Unit II (around 30 to 34 mT) (Fig. 3). In core 02PC, the MDF_{NRM} ranges widely from 25 to 49 mT between the base and 350 cm (Unit II) and is then stable from 350 cm to the top of the core (Units II and I). However, the mean values of those two distinct patterns are similar (30.84 and 29.24 mT, respectively; Fig. 3). MDF_{NRM} values ranging from 25–30 mT suggest the presence of low-coercivity minerals such as magnetite and/or titanomagnetite (Dankers 1981). As the mean pseudo S ratio value in unit II of core 02PC from the base to 350 cm is very stable at 0.94, the higher frequency variations in this interval are likely related to grain size variations of the magnetic grains. In summary, the results indicate that magnetite and/or titanomagnetite is the dominant magnetic mineral throughout the cores under study.

Magnetic grain size and concentration

The NRM_{25-50}, ARM_{25-50}, IRM_{20-50}, and $SIRM_{25-50}$ are significantly higher in Unit I than in Unit II in core 01JPC, suggesting an increase in the concentration of ferrimagnetic minerals (Fig. 3). Unit II is characterized by a weaker k_{ARM}/k_{LF} ratio corresponding to coarser magnetic grains (Fig. 3). The presence of coarser magnetic grains is confirmed by the k_{ARM} vs k_{LF} diagram with the presence of magnetite at <0.1 µm for Unit I and at 0.1 to 5 µm for Unit II (Fig. 4C). Even though these reference lines were obtained for synthetic magnetite grains, they are useful to identify different sedimentary units. Furthermore, the Mrs/Ms and Hcr/Hc values between 0.1–0.3 and 2–5, respectively, match the pseudo-single domain (PSD) magnetite (Day *et al.* 1977; Dunlop 2002a, b) (Fig. 4B).

NRM_{25-50}, ARM_{25-50}, IRM_{20-50}, and $SIRM_{25-50}$ in core 03PC are quite constant in Unit III and show several peaks in Units II and I associated with higher k_{LF} values corresponding to higher concentrations of ferrimagnetic minerals (Fig. 3). The k_{ARM}/k_{LF} ratio increases up-core, suggesting finer magnetic grains (Fig. 3). Although concentrations of ferrimagnetic minerals vary throughout the core, the k_{ARM} vs k_{LF} diagram indicates the presence of magnetite <0.1 µm for Units I and II and between 0.1 to 5 µm for Unit

III (Fig. 4C). The Mrs/Ms and Hcr/Hc ratios for core 03PC are related to a finer magnetic grain size (PSD range) (Fig. 4B).

The k_{ARM}/k_{LF} ratio for core 02PC is higher in Unit I compared to Unit II and is quite constant in Unit II, corresponding to coarser magnetic grains. The magnetic concentration parameters increase during IRD intervals 1 and 2, associated with a slight decrease in the k_{ARM}/k_{LF} ratio (Fig. 3). These results imply higher magnetic concentrations associated with finer magnetic grain size than in the remainder of Unit I. According to the k_{ARM} vs k_{LF} diagram, Unit I sediments are related to magnetite grains smaller than 0.1 μm, whereas sediments from Unit I are related to magnetic grains larger than 5 μm. Sediments from IRD intervals 1 and 2 show a wide scattering in the 0.1 to 5 μm range (Fig. 4C). The hysteresis curves and the Day plot indicate that the magnetic mineralogy of Units I and II is mostly dominated by PSD magnetite. One sample in IRD interval 1 is related to a mixture of single-domain/multi-domain (SD-MD) grains (Fig. 4B).

Natural remanent magnetization

The vector end-point diagrams (Zijderveld 1967) reveal two magnetic components: a viscous remanent magnetization component, easily removed after demagnetization at 10 mT for cores 02PC and 03PC and 5 mT for core 01JPC, and a strong, stable characteristic remanent magnetization (ChRM) (Fig. S4).

The maximum angular deviation (MAD) values are lower than 5° in Unit I in all cores and increase to around 15° in Unit II in core 01JPC. In core 02PC, the MAD values reach a maximum around 40° in Unit II, but are lower than 5° from the end of IRD interval 2 (around 350 cm) to the top of the core (Fig. 5). In core 03PC, the MAD values are lower than 5° for most of the core and increase to around 8° at around 380 cm, which is still indicative of good-quality data (Stoner & St-Onge 2007). Furthermore, the ChRM is expected to fluctuate around the inclination based on a geocentric axial dipole (GAD) model for the coring site latitude, which is 80° for cores 03PC and 02PC and 81.2° for core 01JPC (Fig. 5). To summarize, the three sediment cores are characterized by a strong, well-defined ChRM carried by low-coercivity PSD magnetite, except in the coarser intervals of unit II in cores 01JPC and 02PC and at section breaks for all cores (highlighted areas in Fig. 5). The IRDs intervals in core 02PC are strongly affected by the higher magnetic concentration (shown by k_{LF}; Fig. 3) and the coarser magnetic grain (shown by k_{ARM} vs k_{LF} diagram; Fig. 4C). These coarser intervals were not used in our PSV and RPI reconstructions.

Relative palaeointensity (RPI) determination

According to multiple studies (Levi & Banerjee 1976; Tauxe 1993; Tauxe & Yamazaki 2007), several criteria must be satisfied to validate the reliability of the RPI proxies. The NRM must be characterized by a strong, stable SD-PSD component magnetization carried by magnetite in the 1–15 µm grain-size range. In order to determine the RPI, the NRM should be normalized by an appropriate magnetic parameter to compensate for the variation in ferrimagnetic mineral concentrations. The RPI cannot be correlated with its normalizer or with any of the lithological proxies. Based on the results in the sections above, the required criteria for RPI reconstruction have been fulfilled for cores under study.

The average of the demagnetization steps of 25 to 50 mT (6 steps) for core HLY01 and 20 to 50 mT (7 steps) for cores 03PC and 02PC was used for ARM and IRM as normalizers (Fig. 6B). k_{LF} was not used here because it is not only influenced by concentration and grain-size changes, but also by coarse MD grains, and by both diamagnetic and paramagnetic material. In order to identify the correct normalizer, two different normalization methods were compared for each palaeointensity estimate. The average ratio method is widely used (Channell *et al.* 1997, 2000; Stoner *et al.* 2000; St-Onge *et al.* 2003), and is built by averaging the normalized NRM at different demagnetization steps. The pseudo-Thellier method or the slope method (Tauxe *et al.* 1995; Channell 2002; Snowball & Sandgren 2004; Xuan & Channell 2010) uses the slope of the NRM versus the normalizer at different demagnetization steps. The two methods give similar results for NRM/ARM (Fig. 6A), and the NRM/IRM (not shown). The correlation coefficients (r) calculated from the slope method are high, except for Unit II in core 02PC.

For core 01JPC, the ARM and IRM as normalizers show the same variations for both methods, suggesting that the ARM and the IRM activate the same magnetic assemblages (Fig. 6A, B). The difference between ARM and IRM as normalizers is highlighted in Fig. 6A. These differences occur between 100 and 300 cm in core 03PC and in the IRD intervals in core 02PC, and thus indicate that the grains acquiring the ARM more closely match the coercivity of the grains carrying the NRM. This is also illustrated by looking at the demagnetization behaviour of NRM, ARM, and IRM for the sedimentary record, where ARM better matches the coercivity spectra of the NRM than IRM (Fig. 6B).

The $NRM/ARM_{25\text{-}50}$ mT are not correlated with the ARM ($r^2 = 0.01$) for core 01JPC (Fig. 6C). Comparatively, the $NRM/ARM_{20\text{-}50}$ mT in core 03PC shows a correlation in Unit III ($r^2 = 0.63$) but not in the remaining sediment ($r^2 = 0.22$) (Fig. 6C). For 02PC, the ratio $NRM/ARM_{20\text{-}50}$ mT did not show any correlation with the normalizer in Unit I ($r^2 < 0.004$) but does show a correlation in Unit II ($r^2 < 0.73$) (Fig. 6C). The RPI calculated between 300 and 100 cm in core 03PC and during the IRD intervals in cores 02PC are correlated with the normalized parameter (ARM), indicating the RPI cannot be used to determine chronostratigraphic markers at these intervals.

Finally, ARM was chosen as the preferred normalizer for cores 03PC and 02PC for reasons described below, and for core 01JPC based on its potential to activate only SD and PSD grains (Levi & Banerjee 1976).

Magnetic properties of the sediments in the Chukchi and Beaufort seas

To illustrate the variability of the magnetic properties along a west-east transect from the Chukchi Sea to the Beaufort Sea, they are primarily plotted as a box plot (Fig. S5). Among the most visible patterns, the pseudo S-ratio (hematite-magnetite proportion) is close to 1 along the North American margin for both the Holocene and deglacial intervals. The second pattern is linked to the grain size. The NRM_{25-50}, ARM_{25-50} and k_{ARM}/k_{LF} (magnetic grain size and concentration) mean values are quite similar between the Chukchi and Beaufort seas for the deglacial sediments (NRM: 2.2 10^{-2} *vs* 1.9 10^{-2} A m^{-1}, ARM: 0.9 10^{-2} *vs* 1.1 10^{-2} A m^{-1}, k_{ARM}/k_{LF}: 4 *vs* 3.5 respectively), whereas, mean Holocene values are higher for the Chukchi Sea than the Beaufort Sea (Fig. S5).

The box plot shows that magnetic grain size displayed strong variation since the last deglaciation. The magnetic grain size (k_{ARM}/k_{LF} ratio) decreases generally from the deglacial unit to the Holocene in cores located both at the Beaufort and Chukchi margins (Fig. 7). However, some differences are discernable between the cores. The k_{ARM}/k_{LF} ratio increases respectively from 4 to 15 and from 4 to 50 in cores from the shallowest (05JPC and 08JPC) and deepest (06JPC and 01JPC) Chukchi Sea sites. Comparatively, the k_{ARM}/k_{LF} ratio increases from 4 to 10 in all cores from the Beaufort margin. These observations imply (i) similar magnetic grain size during the deglaciation at both margins, (ii) coarser magnetic grains for the deeper coring sites and finer magnetic grains for the shallower sites at the Chukchi margin during the Holocene, and (iii) generally coarser magnetic grains at the Beaufort margin during the Holocene.

Discussion

Palaeomagnetic dating

Establishing chronostratigraphy in the Arctic is challenging, but the combined use of radiocarbon dating with PSV, relative palaeointensity and geomagnetic field model outputs offers a step forward (Barletta *et al.* 2010; St-Onge & Stoner 2011). The PSV and relative palaeointensity records of cores 01JPC, 03PC, and 02PC were compared with the prior palaeomagnetic records from the Chukchi (05JPC, 06JPC, 08JPC, 16JPC; Barletta *et al.* 2008; Lisé-Pronovost *et al.* 2009; Darby *et al.* 2012; Lund *et al.* 2016) and Beaufort seas (803PC, 650PC; Barletta *et al.* 2008, 2010) (Fig. 9). The chronology of these cores was determined using a combination of radiocarbon ages with palaeomagnetic tie points and corroborated by geomagnetic model outputs (Table S1). All these cores show similar directional and relative palaeointensity features that can be correlated on a regional scale. Cores 803PC and 05JPC were also used to add tie points for the age model of core 16JPC (Darby *et al.* 2012).

Our records show similarities with other marine records from the Chukchi and Beaufort seas and also with the CALS10k model output for the latitude of the site (Korte *et al.* 2011), and allow for an identification of 22 tie-points in total (Fig. 9, Table 3). Nine tie points have been identified in this study, including 9 common features for inclination, 6 common features for declination, and 7 RPI common features. Four of the inclination tie-points, I2 to I5, have been used in earlier studies for the inclination records between 2000 and 5800 cal. a BP (Lisé-Pronovost *et al*. 2009; Barletta *et al*. 2010b). Two of the declination features have also been observed in the Chukchi cores, one minimum (D4: 4900 cal. a BP) and a maximum (D5: 5950 cal. a BP) in Barletta *et al.* (2010) and Lisé-Pronovost *et al.* (2009). Furthermore, RPI tie point P6 was used in Lisé-Pronovost *et al*. (2009) for cores from the Chukchi margin. All tie points are presented in Table 3, and the mean and standard deviation ages (1σ) were calculated using the age of the identified tie points for the comparative cores.

Age modelling

Age models were first generated using the non-palaeomagnetic data: ^{14}C ages in cores 02JPC and 03JPC from the Beaufort Sea and the tephra peak in core 01JPC from the Chukchi Sea (Fig. 8A), and then improved by adding palaeomagnetic tie points (Fig. 8B). A constant linear sedimentation rate of 65 cm ka^{-1} was assumed for the lithologically homogenous, ~300-cm long upper unit of 01JPC based on the ^{210}Pb data from 01MC (Fig. 8A). This initial age model was then improved using a stratigraphy-based

Bayesian approach with Bacon (Blaauw & Christen 2011) and the palaeomagnetic tie points (Fig. 8B). The D5-A tie point was excluded as an outlier based on the comparison of tie-point positions with the linear age model (Fig. 8A). The resulting composite age-depth model for core 01JPC shows that the Holocene (Unit I) sediment record spans the last 6000 years, with sedimentation rates averaging 60 cm ka^{-1} (Fig. 8B). This number is very close to the sedimentation rate of 65 cm ka^{-1} estimated from the ^{210}Pb data in 01MC that shows a clear exponential decrease (Fig. S3). Based on age model (Fig. 8B), the top age of core 01TWC is estimated around 1000 cal. a BP, implying missing sediment at the top. This conclusion is consistent with the diffuse spectral reflectance data (L*, a* and b*) that does not show any visible correlations in both the absolute values and relative variations between 01TWC and the 45-cm-long 01MC (Fig. S2). Assuming a top age of 1000 cal. a BP for core 01TWC and sedimentation rates between 60 and 65 cm ka^{-1}, the thickness of missing sediment is 60-65 cm.

Another implication of the age model above is that the base of the marine Unit I in core 01JPC has an age of around 6000 cal. a BP, considerably younger than previously investigated cores from the study area (Darby *et al.* 2009, 2012; Lisé-Pronovost *et al.* 2009; Polyak *et al.* 2016), which suggests a hiatus in the bottom part of the Holocene. The absence of tephra related to the ~7000 cal. a BP prominent Kamchatka KS_2 eruption in 01JPC is consistent with an early Holocene hiatus in this core (V. Ponomavera, pers. comm. 2016). Furthermore, a similar hiatus of several ka duration has been identified in a well-dated sediment record from the Herald Canyon at the western (Siberian) part of the Chukchi margin (Pearce *et al.* 2016). Considering the absence of the 01JPC hiatus in nearby cores, it has to be associated with local bottom processes rather than with a regional halt in sedimentation. As this core is located in or close to a canyon in the lower part of the slope (Fig. 1), a disruption of normal sedimentation is not unlikely, and could be related to either downslope sediment movement (slump, debris flow or turbidite) or a winnowing/nondeposition by downwelling waters. The latter explanation is more plausible since no apparent erosional surface is visible at the level of the inferred hiatus. According to modern hydrographic observations, dense waters (brines) generated at the Chukchi-Alaskan margin during the fall/winter sea-ice formation can descend to the pycnocline depth of up to 200 m (Pickart *et al.* 2005; Woodgate *et al.* 2005). However, geochemical data from bottom sediments from the adjacent slope and deep-sea basin indicate the possibility of a much deeper convection in the recent past (Haley & Polyak 2013). While this issue requires further investigation, the occurrence of a lower Holocene hiatus in cores from the Chukchi slope may indicate more intense sea-ice and brine formation during that time, possibly related to the flooding of Siberian shelves by rising postglacial sea level as predicted by numeric modelling experiments (Blaschek & Renssen 2013).

The preliminary age models for the Beaufort Sea cores 03PC and 02PC (Fig. 8A) were constructed using radiocarbon ages including the new radiocarbon dates and ages from nearby core 750PC correlated to the cores under study using the IRD layers as described above. Apparently outlying (by ~300 years: Fig. 8A) palaeomagnetic tie points D6 and I7 were excluded from the construction of a more comprehensive age model for both cores. Tie point I1 was also excluded from the age model for core 03PC, as well as tie points P1, P5 and P6 for core 02PC for being a bit outside or on the 95% confidence limit (Fig. 8A). A composite age model was then constructed for both cores based on the palaeomagnetic tie points and radiocarbon ages (Fig. 8B). The resulting age model for 02JPC spans the last 13 500 years and displays a considerable variation in sedimentation rates with a rapid decrease from 60 to 10-20 cm ka^{-1} at the deglacial/Holocene transition. These results are similar to sedimentation patterns in core 750PC, with sedimentation rates of 15 cm ka^{-1} estimated for the Holocene (Scott *et al.* 2009). The composite age model for 03JPC indicates that this core spans the last 10 500 years and is associated with sedimentation rates averaging ~70 cm ka^{-1} between 6 000 and 8 000 cal. a BP and ~40-

45 cm ka^{-1} above and below this interval (Fig. 8B). Core 03PC is the first complete marine succesion recording palaeomagnetic secular variations for the entire Holocene from the Beaufort Sea.

Limits of the palaeomagnetic reconstructions

Sedimentation rates play an important role in the temporal resolution of palaeomagnetic records. The Chukchi Sea cores used for a comparison with cores under study have sedimentation rates as high as >100 cm ka^{-1}, probably in relation to a proximity to the Barrow Canyon, a major conduit of sediment for the eastern Chukchi margin. The temporal resolution of cores studied in this paper is lower due to a more distal location from sediment sources (Barrow Canyon and Mackenzie delta; Fig. 1). Furthermore, the 7 cm smoothing effect of the cryogenic magnetometer combined with lower sedimentation rates may have impaired the identification of common features between the cores, as shown in Fig. 9. Indeed, based on the Holocene sedimentation rates derived from cores 01JPC, 03PC and 02PC, the 7 cm smoothing effect of the response function of the magnetometer creates a smoothing of respectively 115, 100-175 and 350-700 years. This is especially evident in core 02PC, where the temporal resolution of the PSV profile is lower than in other cores, allowing us to identify only 3 common features in the inclination and declination profiles (Fig. 9). Nevertheless, the surface sediment of this core represents modern sediments, and the uppermost IRD layer can be identified and dated to 11 580 cal. a BP (Scott *et al.* 2009), which enables a reliable age framework for this core. In addition, most of the tie points identified are within the 95% confidence limit (<300 years off the center line) of the age model based on ^{14}C ages (Fig. 8A). Only tie points D6 and I7 showed a higher offset in both cores 03PC and 02PC (Table 3).

Palaeomagnetic records with greigite as the main magnetic mineral need to be interpreted with caution, as their PSV and relative palaeointensity variations can be biased and reflects rock magnetic properties rather than geomagnetic variations (Ron *et al.* 2007). In cores used in this study or for the comparison, greigite was found only in core HLY05 at restricted intervals (Brachfeld *et al.* 2009).

Furthermore, the small presence of greigite in that core is not likely to compromise the palaeomagnetic data as the remanence is still carried by the low coercivity minerals such as magnetite (Barletta *et al.* 2008; Brachfeld *et al.* 2009; Lisé-Pronovost *et al.* 2009). The pseudo S-ratio, hysteresis curves and the Day plots for cores 06JPC, 08JPC and 650PC indicate a magnetic assemblage dominated by magnetite but not iron sulphides, such as greigite (Lisé-Pronovost *et al.* 2009; Barletta *et al.* 2010). In addition, the presence of greigite was not detected in cores under study using XRD (Fig. S7), and magnetite was found to be the dominant magnetic mineral and none greigite was found in surface sediments from the Beaufort Sea (Gamboa *et al.* 2017). As described in the magnetic mineralogy section, the hysteresis curves, pseudo-S ratio, and MDF_{NRM}, as well as the low MAD values are characteristic of low-coercivity ferrimagnetic minerals, such as magnetite, yielding reliable PSV data reconstruction (Tauxe *et al.* 1996). The magnetic results presented in this study are similar to those published in Lisé-Pronovost *et al*. (2009), Barletta *et al*. (2010), and Darby *et al.* (2009). In addition, the influence of reductive diagenesis can be measured by the ratio Fe/k_{LF} (Funk 2004; Hofmann *et al.* 2005; Hofmann & Fabian 2007, 2009). For the studied cores, the mean Fe/k_{LF} ratio varies around 18-20 (Fig. S6). According to Funk (2004) and Hofmann *et al.* (2005), a Fe/k_{LF} ratio under 40 is indicative of weak reductive diagenesis. Based on the Fe/k_{LF} ratio and the magnetic properties, the data, thus, clearly indicate that the remanence is principally carried by low coercivity minerals, such as magnetite.

Sedimentation rates in the Canadian Beaufort Sea

As shown in Fig. 9, sedimentation rates in cores from the Beaufort Sea are heavily dependent on their location, with the largest difference in sedimentation patterns observed between the eastern Beaufort Sea and the Mackenzie delta. Before 11 500 cal. a BP, sedimentation rates were higher than 60 cm ka^{-1} in both areas, likely due to higher input of the Mackenzie River and also meltwater discharge from the Laurentide Ice Sheet (Schell *et al*. 2008). After 11 500 cal. a BP, sedimentation rates were still high in the Mackenzie area (>40 cm ka^{-1}), but lower in the eastern Beaufort sea (10-20 cm ka^{-1}). Indeed, the age-model curve of core 02PC is very similar to the relative sea-level curves from the Mackenzie delta area (Fig. 10; Hill *et al.* 1993; Héquette *et al.* 1995). The rate of sea-level rise between 9000 and 3000 cal. a BP was 700–1400 cm ka^{-1}, followed by a decrease to 200 cm ka^{-1} since 3000 cal. a BP, resulted in high rates of coastal retreat that had a strong effect on the Mackenzie delta (Héquette *et al.* 1995). Sediment inputs from the Mackenzie delta are still very high in the Mackenzie Trough while they seems to be influenced by sea-level variation in the eastern Beaufort Sea (as shown by core 02PC) during the Holocene.

Magnetic properties of the sediments on the Arctic North American margin

The three new sediment cores considerably expand the data on magnetic properties from prior studies performed on sediment cores from the Chukchi and Beaufort seas (Barletta *et al.* 2008, 2010; Lisé-Pronovost *et al.* 2009; Lund *et al.* 2016). As shown in Fig. S5 for cores under study, the pseudo S-ratio close to 1 and the Mrs/Ms and Hcr/Hc ratios typical for low-coercivity ferrimagnetic grains indicate that magnetite in the PSD grain range is the dominant magnetic mineral on the North American margin.

As described previously, (i) the magnetic grain size was similarly high during deglaciation at both the Chukchi and Beaufort Sea margins, (ii) the Holocene magnetic grains at the Chukchi margin are coarser at shallower water depths, and (iii) during the Holocene magnetic grains are generally coarser at the Beaufort margin (Fig. 7). The magnetic grain size in the Chukchi Sea cores ranged between 4 to 16 µm (Barletta *et al.* 2008; Lisé-Pronovost *et al.* 2009; this study). This range of magnetic grain size matched the granulometry mode centered at 7 µm and characteristic from glacial environment found in Dong *et al.* (2017). Furthermore, coarse magnetic grain size during the deglaciation co-occurs with the high contents of IRD at the Chukchi and Beaufort margins reflecting predominant sedimentation from icebergs (Polyak *et al.* 2007; Scott *et al.* 2009). For example, the coarse magnetic grain size presented in this study correlates with high IRD contents and Fe-oxide grains with the Canadian Arctic Archipelago source in the core P2 from the Chukchi margin (Polyak *et al.* 2007). The Canadian Arctic Archipelago is characterized by high content of magnetite and titanomagnetite and were entrained by icebergs from the Laurentide and Innuitian ice sheets during the deglacial (Bischof & Darby 1999). These IRD pulses from the Canadian Arctic Archipelago have been linked to the deglacial discharge from the Laurentide ice sheet, primarily via the Amundsen Gulf and M'Clure Strait (Stokes *et al.* 2005, 2006). We suggest that glacial erosion and meltwater from the Laurentide Ice Sheet induced higher mechanical weathering and enhanced the transport of coarser magnetic and titomagnetique grains by IRD to the Beaufort and Chukchi seas. With the cessation of Laurentide Ice Sheet meltwater and iceberg inputs, numbers of IRD strongly decreased in the Holocene sediments at both margins.

During the Holocene the eastern Beaufort Sea cores (02PC and 03PC) was under a strong, direct influence of the detrital material from the Mackenzie River (Schell *et al.* 2008; Darby *et al.* 2009; Scott *et al.* 2009). The Chukchi margin sedimentation in the Holocene was presumably predominated by transport by currents from the adjacent shelf and deposition from sea ice (Darby *et al.* 2009). The magnetic grain size in the Chukchi Sea cores ranges between 0.1 and 4 µm (Barletta *et al.* 2008; Lisé-Pronovost *et al.* 2009; this study). This range of magnetic grain size matches the granulometry mode centered at ~4 µm in interglacial sediments in the Arctic Ocean interpreted as a combination of deposition from sea ice and from suspension, possibly resulting from winnowing of the fine particles (Dong *et al.* 2017). Deposition from sea ice alone implies a generally uniform grain size distribution across the study area, which does not seem to be the case for the studied cores, where magnetic grains are finer and coarser at deeper and shallower sites, respectively. We, therefore, infer that cross-shelf and/or downslope currents had a major control on the Holocene sedimentation in the cores located close to the head of the Barrow Canyon, where currents average about 14 cm s^{-1} and can reach nearly 100 cm

s^{-1} (Darby *et al.* 2009). The upwelling currents along the slope might mix with the down-canyon flows to create eddies or decrease net currents thus promoting deposition (Darby *et al.* 2009). In this setting, the current impact decreased downslope, consistent with the observed preferential redeposition of fine grains at deeper sites. Bottom currents may therefore account for the magnetic grain size differences between cores from the shelf (08JPC) and from deeper sites on the adjacent slope (01JPC, 06JPC). However, we cannot exclude sea ice as an additional mechanism for transporting finer magnetic grains to the deeper sites, especially considering their geographic proximity to the position of sea-ice margin suggested for a considerable part of the Holocene (Polyak *et al.* 2016).

Conclusions

The natural remanent magnetization of sediments from the Chukchi and Beaufort Sea margins is characterized by a strong, well-defined, stable single component magnetization carried by single to pseudo-single domain magnetite, thus highlighting the quality of palaeomagnetic data for sediment cores from this area. This paper presents three new records of the Holocene palaeomagnetic secular variations and relative palaeointensity in sediment cores from the Chukchi and Beaufort margins, including the first full vector data for the entire Holocene in the Beaufort Sea (cores 02PC and 03PC). These data enabled us to construct age models for both areas, where obtaining radiocarbon ages are complicated by a scarcity of biogenic calcareous material suitable for dating. Previously reported regional palaeomagnetic records helped to constrain the chronology of cores under this study. The age model derived from magnetostratigraphy was verified by independent dating techniques such as radiocarbon in cores 02PC and 03PC, and ^{210}Pb and tephrochronology in 01JPC. Our results for the Beaufort margin cores illustrate a large difference in resolution for the Holocene records related to a decrease in sedimentation rates away from the Mackenzie River delta, which is an important factor that needs to be considered in regional palaeoceanographic investigations.

The presented data also suggest that deposition of coarse magnetic grains in the lower part of the stratigraphy was controlled by high IRD inputs from the Laurentide Ice Sheet during deglaciation throughout both the Beaufort and Chukchi margins. In the Holocene deposits, a higher variability in magnetic parameters is observed in cores from the Chukchi margin, where finer magnetic grains characterize larger water depths, presumably in relation to a bottom current control.

Overall, this study illustrates the usefulness of palaeomagnetism to improve the dating of Arctic geological material, as well as regional and global geomagnetic field models.

Acknowledgments. – We sincerely thank the captains, officers, crew and scientists on board the USCGC Healy and the CCGS Amundsen for the recovery the cores used in this study. These cores were collected as part of the HOTRAX expedition (USCGC Healy), as well as the CASES and ArcticNet (CCGS Amundsen) programs. We also thank Quentin Beauvais (ISMER), Mathieu Babin (ISMER), and Bassam Ghaleb (UQAM-GEOTOP) for their technical support and advice in the laboratory. We would also like to thank Steve Lund (University of South California, Los Angeles, USA) for sharing the PSV data of the core 16JPC. This research was funded by the Natural Sciences and Engineering Research Council of Canada (NSERC) through Discovery Grants to G. St-Onge and J-C Montero-Serrano, as well as through ship time support for several expeditions (J.-C. Montero-Serrano, G. St-Onge). L. Polyak's contribution was supported by the US National Science Foundation award ARC-0612493. Finally, we thank Christine Laurin for reviewing the grammar as well as the editor Jan A. Piotrowski and the reviewers Dennis A. Darby and Daniel Rey for their constructive comments that helped improved the manuscript.

References

Andrews, J. T. & Dunhill, G. 2004: Early to mid-Holocene Atlantic water influx and deglacial meltwater events, Beaufort Sea slope, Arctic Ocean. *Quaternary Research 61*, 14-21.

Asahara, Y., Takeuchi, F., Nagashima, K., Harada, N., Yamamoto, K., Oguri, K. & Tadai, O. 2012: Provenance of terrigenous detritus of the surface sediments in the Bering and Chukchi Seas as derived from Sr and Nd isotopes: Implications for recent climate change in the Arctic regions. *Deep-Sea Research Part II: Topical Studies in Oceanography 61-64*, 155-171.

Barletta, F., St-Onge, G., Channell, J. E. T. & Rochon, A. 2010: Dating of Holocene western Canadian Arctic sediments by matching paleomagnetic secular variation to a geomagnetic field model. *Quaternary Science Reviews 29*, 2315-2324.

Barletta, F., St-Onge, G., Channell, J. E. T., Rochon, A., Polyak, L. & Darby, D. 2008: High-resolution paleomagnetic secular variation and relative paleointensity records from the western Canadian Arctic: implication for Holocene stratigraphy and geomagnetic field behaviour. *Canadian Journal of Earth Sciences 45*, 1265-1281.

Bischof, J. F. & Darby, D. A. 1999: Quaternary ice transport in the Canadian Arctic and extent of Late Wisconsinan Glaciation in the Queen Elizabeth Islands. *Canadian Journal of Earth Sciences 36*, 2007-2020.

Blaauw, M. 2010: Methods and code for 'classical' age-modelling of radiocarbon sequences. *Quaternary Geochronology 5*, 512-518.

Blaauw, M. & Christen, A. 2011: Flexible Paleoclimate Age-Depth Models Using an Autoregressive Gamma Process. *Bayesian Analysis 6*, 457-474.

Blaschek, M. & Renssen, H. 2013: The impact of early holocene arctic shelf flooding on climate in an atmosphere-ocean-sea-ice model. *Climate of the Past 9*, 2651-2667.

Blott, S. J. & Pye, K. 2001: GRADISTAT: A Grain Size Distribution and Statistic Package For the Analysis of Unconsolidated Sediments. *Earth Surface Processes and Landforms 26*, 1237-1248.

Brachfeld, S., Barletta, F., St-Onge, G., Darby, D. & Ortiz, J. D. 2009: Impact of diagenesis on the environmental magnetic record from a Holocene sedimentary sequence from the Chukchi-Alaskan margin, Arctic Ocean. *Global and Planetary Change 68*, 100-114.

Bringué, M. & Rochon, A. 2012: Late Holocene paleoceanography and climate variability over the Mackenzie Slope (Beaufort Sea, Canadian Arctic). *Marine Geology 291-294*, 83-96.

Carson, M. A., Jasper, J. N. & Conly, F. M. 1998: Magnitude and sources of sediment input to the Mackenzie Delta, Northwest Territories, 1974 – 94. *Arctic 51*, 116-124.

Channell, J. E. T. 2002: Geomagnetic excursions and paleointensities in the Matuyama Chron at Ocean Drilling Program Sites 983 and 984 (Iceland Basin). *Journal of Geophysical Research 107*, 2114-2114.

Channell, J. E. T., Hodell, D. A. & Lehman, B. 1997: Relative geomagnetic paleointensity and $\delta^{18}O$ at ODP Site 983 (Gardar Drift, North Atlantic) since 350 ka. *Earth and Planetary Science Letters 153*, 103-118.

Channell, J. E. T., Stoner, J. S., Hodell, D. A. & Charles, C. D. 2000: Geomagnetic paleointensity for the last 100 kyr from the sub-antarctic South Atlantic: A tool for inter-hemispheric correlation. *Earth and Planetary Science Letters 175*, 145-160.

Coulter, S. E., Pilcher, J. R., Plunkett, G., Baillie, M., Hall, V. A., Steffensen, J. P., Vinther, B. M., Clausen, H. B. & Johnsen, S. J. 2012: Holocene tephras highlight complexity of volcanic signals in Greenland ice cores. *Journal of Geophysical Research: Atmospheres 117*, D21303. doi: 10.1029/2012JD017698.

Dankers, P. 1981: Relationship between median destructive field and remanent coercive forces for dispersed natural magnetite, titanomagnetite and hematite. *Geophysical Journal International 64*, 447-461.

Darby & Bischof 2004: A Holocene record of changing Arctic Ocean ice drift analogous to the effects of the Arctic Oscillation. *Paleoceanography 19*, 1-9.

Darby, D. A. 2003: Sources of sediment found in sea ice from the western Arctic Ocean, new insights into processes of entrainment and drift patterns. *Journal of Geophysical Research 108*, 1-10.

Darby, D. A., Ortiz, J., Polyak, L., Lund, S., Jakobsson, M. & Woodgate, R. A. 2009: The role of currents and sea ice in both slowly deposited central Arctic and rapidly deposited Chukchi-Alaskan margin sediments. *Global and Planetary Change 68*, 58-72.

Darby, D. A., Ortiz, J. D., Grosch, C. E. & Lund, S. P. 2012: 1,500-year cycle in the Arctic Oscillation identified in Holocene Arctic sea-ice drift. *Nature Geoscience 5*, 897-900.

Darby, D. A., Polyak, L. & Bauch, H. A. 2006: Past glacial and interglacial conditions in the Arctic Ocean and marginal seas - a review. *Progress in Oceanography 71*, 129-144.

Darby, D., Jakobsson, M., & Polyak, L. 2005. Icebreaker expedition collects key Arctic seafloor and ice data. *EOS 86*, 549-552.

Day, R., Fuller, M. & Schmidt, V. A. 1977: Hysteresis properties of titanomagnetites: Grain-size and compositional dependence. *Physics of the Earth and Planetary Interiors 13*, 260-267.

Debret, M., Sebag, D., Desmet, M., Balsam, W., Copard, Y., Mourier, B., Susperrigui, a. S., Arnaud, F., Bentaleb, I., Chapron, E., Lallier-Vergès, E. & Winiarski, T. 2011: Spectrocolorimetric interpretation of sedimentary dynamics: The new "Q7/4 diagram". *Earth-Science Reviews 109*, 1-19.

Montero-Serrano, J.-C., Deschamps, C.-E., & Jaegle, M. 2014. Amundsen Expedition Report: Geology and paleoceanography leg 2a. ArctiNet, Université Laval, 307-311. http://www.arcticnet.ulaval.ca/pdf/media/2014_Amundsen_Expedition_Report.pdf.

Dong, L., Liu, Y., Shi, X., Polyak, L., Huang, Y., Fang, X., Liu, J., Zou, J., Wang, K., Sun, F. & Wang, X. 2017: Sedimentary record from the Canada Basin, Arctic Ocean: implications for late to middle Pleistocene glacial history. *Climate of the Past 13*, 511-531.

Dunlop, D. J. 2002a: Theory and application of the Day plot (Mrs/Ms versus Hcr/Hc) 2. Application to data for rocks, sediments, and soils. *Journal of Geophysical Research 107*, 2057-2057. doi: 10.1029/2001JB000487.

Dunlop, D. J. 2002b: Theory and application of the Day plot (Mrs/Ms versus Hcr/Hc) 1. Theoretical curves and tests using titanomagnetite data. *Journal of Geophysical Research 107*, 2056-2056. doi: 10.1029/2001JB000486.

Durantou, L., Rochon, A., Ledu, D., Massé, G., Schmidt, S. & Babin, M. 2012: Quantitative reconstruction of sea-surface conditions over the last 150 yr in the Beaufort Sea based on dinoflagellate cyst assemblages: The role of large-scale atmospheric circulation patterns. *Biogeosciences 9*, 5391-5406.

Funk, J. A. 2004: Sediment Accumulation and Diagenesis in the Late Quaternary Equatorial Atlantic Ocean: An Environmental Magnetic and Geochemical Perspective. 98 pp. Universität Bremen, Bremen.

Gamboa, A., Montero-Serrano, J.-C., St-Onge, G., Rochon, A. & Desiage, P.-A. 2017: Mineralogical, geochemical and magnetic signatures of surface sediments from the Canadian Beaufort Shelf and Amundsen Gulf (Canadian Arctic). *Geochemistry, Geophysics, Geosystems 18*, 488-512.

Geiss, C. E. & Banerjee, S. K. 2003: A Holocene-Late Pleistocene geomagnetic inclination record from Grandfather Lake, SW Alaska. *Geophysical Journal International 153*, 497-507.

Hagstrum, J. T. & Champion, D. E. 2002: A Holocene paleosecular variation record from 14C-dated volcanic rocks in western North America. *Journal of Geophysical Research 107*, 2025-2025.

Haley, B. A. & Polyak, L. 2013: Pre-modern Arctic Ocean circulation from surface sediment neodymium isotopes. *Geophysical Research Letters 40*, 893-897.

Hanslik, D., Jakobsson, M., Backman, J., Björck, S., Sellén, E., O'Regan, M., Fornaciari, E. & Skog, G. 2010: Quaternary Arctic Ocean sea ice variations and radiocarbon reservoir age corrections. *Quaternary Science Reviews 29*, 3430-3441.

Héquette, A., Marie-Hélène, R. & Hill, P. R. 1995: The effects of the Holocene Sea Level Rise on the Evolution of the Southeastern Coast of the Canadian Beaufort Sea. *Journal of Coastal Research 11*, 494-507.

Hill, J. C. & Driscoll, N. W. 2008: Paleodrainage on the Chukchi shelf reveals sea level history and meltwater discharge. *Marine Geology 254*, 129-151.

Hill, J. C., Driscoll, N. W., Brigham-Grette, J., Donnelly, J. P., Gayes, P. T. & Keigwin, L. 2007: New evidence for high discharge to the Chukchi shelf since the Last Glacial Maximum. *Quaternary Research 68*, 271-279.

Hill, P. R., Héquette, A. & Ruz, M.-H. 1993: Holocene sea-level history of the Canadian Beaufort shelf. *Canadian Journal of Earth Sciences 30*, 103-108.

Hillaire-Marcel, C., Maccali, J., Not, C. & Poirier, A. 2013: Geochemical and isotopic tracers of Arctic sea ice sources and export with special attention to the Younger Dryas interval. *Quaternary Science Reviews 79*, 184-190.

Hofmann, D. I. & Fabian, K. 2007: Rock magnetic properties and relative paleointensity stack for the last 300 ka based on a stratigraphic network from the subtropical and subantarctic South Atlantic. *Earth and Planetary Science Letters 260*, 297-312.

Hofmann, D. I. & Fabian, K. 2009: Correcting relative paleointensity records for variations in sediment composition: Results from a South Atlantic stratigraphic network. *Earth and Planetary Science Letters 284*, 34-43.

Hofmann, D. I., Fabian, K., Schmieder, F., Donner, B. & Bleil, U. 2005: A stratigraphic network across the Subtropical Front in the central South Atlantic: Multi-parameter correlation of magnetic susceptibility, density, X-ray fluorescence and $\delta^{18}O$ records. *Earth and Planetary Science Letters 240*, 694-709.

Kaufman, D. S., Jensen, B. J. L., Reyes, A. V., Schiff, C. J., Froese, D. G. & Pearce, N. J. G. 2012: Late Quaternary tephrostratigraphy, Ahklun Mountains, SW Alaska. *Journal of Quaternary Science 27*, 344-359.

Keigwin, L. D., Donnelly, J. P., Cook, M. S., Driscoll, N. W. & Brigham-Grette, J. 2006: Rapid sea-level rise and Holocene climate in the Chukchi Sea. *Geology 34*, 861-864.

Kirschvink, J. L. 1980: The least-squares line and plane and the analysis of palaeomagnetic data. *Geophysical Journal International 62*, 699-718.

Korte, M., Constable, C., Donadini, F. & Holme, R. 2011: Reconstructing the Holocene geomagnetic field. *Earth and Planetary Science Letters 312*, 497-505.

Korte, M. & Constable, C. G. 2005: The geomagnetic dipole moment over the last 7000 years—new results from a global model. *Earth and Planetary Science Letters 236*, 348-358.

Ledu, D., Rochon, A., de Vernal, A. & St-Onge, G. 2008: Palynological evidence of Holocene climate change in the eastern Arctic: a possible shift in the Arctic oscillation at the millennial time scale. *Canadian Journal of Earth Sciences 45*, 1363-1375.

Levi, S. & Banerjee, S. K. 1976: On the possibility of obtaining relative paleointensities from lake sediments. *Earth and Planetary Science Letters 29*, 219-226.

Lisé-Pronovost, A., St-Onge, G., Brachfeld, S., Barletta, F. & Darby, D. 2009: Paleomagnetic constraints on the Holocene stratigraphy of the Arctic Alaskan margin. *Global and Planetary Change 68*, 85-99.

Lund, S., Keigwin, L. & Darby, D. 2016: Character of Holocene paleomagnetic secular variation in the tangent cylinder: Evidence from the Chukchi Sea. *Physics of the Earth and Planetary Interiors 256*, 49-58.

Matthiessen, J., Kunz-Pirrung, M. & Mudie, P. J. 2000: Freshwater chlorophycean algae in recent marine sediments ofthe Beaufort, Laptev and Kara Seas (Arctic Ocean) as indicators of river runoff. *International Journal of Earth Sciences 89*, 470-485.

Mazaud, A. 2005: User-friendly software for vector analysis of the magnetization of long sediment cores. *Geochemistry, Geophysics, Geosystems 6*, Q12006. doi: 10.1029/2005GC001036.

McKay, J. L., de Vernal, A., Hillaire-Marcel, C., Not, C., Polyak, L. & Darby, D. 2008: Holocene fluctuations in Arctic sea-ice cover: dinocyst-based reconstructions for the eastern Chukchi Sea. *Canadian Journal of Earth Sciences 45*, 1377-1397.

McNeely, R., Dyke, A. S. & Southon, J. R. 2006: Canadian marine reservoir ages, preliminary data assessment, Geological Survey of Canada, Open File 5049. doi: 10.13140/2.1.1461.6649.

O'Brien, M. C., Macdonald, R. W., Melling, H. & Iseki, K. 2006: Particle fluxes and geochemistry on the Canadian Beaufort Shelf: Implications for sediment transport and deposition. *Continental Shelf Research 26*, 41-81.

Ortiz, J. D., Polyak, L., Grebmeier, J. M., Darby, D., Eberl, D. D., Naidu, S. & Nof, D. 2009: Provenance of Holocene sediment on the Chukchi-Alaskan margin based on combined diffuse spectral reflectance and quantitative X-Ray Diffraction analysis. *Global and Planetary Change 68*, 73-84.

Pearce, C., Varhelyi, A., Wastegård, S., Muschitiello, F., Barrientos, N., O'Regan, M., Cronin, T., Gemery, L., Semiletov, I., Backman, J. & Jakobsson, M. 2016: The 3.6 ka Aniakchak tephra in the Arctic Ocean: a constraint on the Holocene radiocarbon reservoir age in the Chukchi Sea. *Climate of the Past Discussions 13*, 303-316.

Pearce, N. J. G., Westgate, J. A., Preece, S. J., Eastwood, W. J. & Perkins, W. T. 2004: Identification of Aniakchak (Alaska) tephra in Greenland ice core challenges the 1645 BC date for Minoan eruption of Santorini. *Geochemistry, Geophysics, Geosystems 5*, Q03005. doi: 10.1029/2003GC000672.

Phillips, R. L. & Grantz, A. 2001: Regional variations in provenance and abundance of ice-rafted clasts in Arctic Ocean sediments: Implications for the configuration of late Quaternary oceanic and atmospheric circulation in the Arctic. *Marine Geology 172*, 91-115.

Pickart, R. S. 2004: Shelfbreak circulation in the Alaskan Beaufort Sea: Mean structure and variability. *Journal of Geophysical Research C: Oceans 109*, 1-14.

Pickart, R. S., Weingartner, T. J., Pratt, L. J., Zimmermann, S. & Torres, D. J. 2005: Flow of winter-transformed Pacific water into the Western Arctic. *Deep-Sea Research Part II: Topical Studies in Oceanography 52*, 3175-3198.

Polyak, L., Belt, S. T., Cabedo-Sanz, P., Yamamoto, M. & Park, Y. H. 2016: Holocene sea-ice conditions and circulation at the Chukchi-Alaskan margin, Arctic Ocean, inferred from biomarker proxies. *The Holocene 26*, 1810-1821.

Polyak, L., Bischof, J., Ortiz, J. D., Darby, D. A., Channell, J. E. T., Xuan, C., Kaufman, D. S., Løvlie, R., Schneider, D. A., Eberl, D. D., Adler, R. E. & Council, E. A. 2009: Late Quaternary stratigraphy and sedimentation patterns in the western Arctic Ocean. *Global and Planetary Change 68*, 5-17.

Polyak, L., Darby, D. A., Bischof, J. F. & Jakobsson, M. 2007: Stratigraphic constraints on late Pleistocene glacial erosion and deglaciation of the Chukchi margin, Arctic Ocean. *Quaternary Research 67*, 234-245.

Ponomareva, V., Polyak, L., Portnyagin, M., Abbott, P. & Davies, S. 2014: A Holocene cryptotephra record from the Chukchi margin: the first tephrostratigraphic study in the Arctic Ocean. Presented at *PAST* Gateways International Conference and Workshop, Trieste, Italy.

Pyne-O'Donnell, S. 2011: The taphonomy of Last Glacial-Interglacial Transition (LGIT) distal volcanic ash in small Scottish lakes. *Boreas 40*, 131-145.

Reimer, P. J., Bard, E., Bayliss, A., Beck, J. W., Blackwell, P. G., Ramsey, C. B., Buck, C. E., Cheng, H., Edwards, R. L., Friedrich, M., Grootes, P. M., Guilderson, T. P., Haflidison, H., Hajdas, I., Hatté, C., Heaton, T., Hoffmann, D. L., Hogg, A., Hughen, K. A., Kaiser, K., Kromer, B., Manning, S. W., Niu, M., Reimer, R., Richards, D. A., Scott, E. M., Southon, J. R., Staff, R. A., Turney, C. & Plicht, J. 2013: IntCal13 and Marine13 radiocarbon age calibration curves 0-50,000 years cal BP. *Radiocarbon 55*, 1869-1887.

Richerol, T., Rochon, A., Blasco, S., Scott, D. B., Schell, T. M. & Bennett, R. J. 2008: Distribution of dinoflagellate cysts in surface sediments of the Mackenzie Shelf and Amundsen Gulf, Beaufort Sea (Canada). *Journal of Marine Systems 74*, 825-839.

Ron, H., Nowaczyk, N. R., Frank, U., Schwab, M. J., Naumann, R., Striewski, B. & Agnon, a. 2007: Greigite detected as dominating remanence carrier in Late Pleistocene sediments, Lisan formation, from Lake Kinneret (Sea of Galilee), Israel. *Geophysical Journal International 170*, 117-131.

Schell, T. M., Scott, D. B., Rochon, A. & Blasco, S. 2008: Late Quaternary paleoceanography and paleo-sea ice conditions in the Mackenzie Trough and Canyon, Beaufort Sea. *Canadian Journal of Earth Sciences 45*, 1399-1415.

Scott, D. B., Schell, T., St-Onge, G., Rochon, A. & Blasco, S. 2009: Foraminiferal assemblage changes over the last 15,000 years on the Mackenzie-Beaufort Sea Slope and Amundsen Gulf, Canada: Implications for past sea ice conditions. *Paleoceanography 24*, 1-20.

Snowball, I. & Sandgren, P. 2004: Geomagnetic field intensity changes in Sweden between 9000 and 450 cal BP: extending the record of "archaeomagnetic jerks" by means of lake sediments and the pseudo-Thellier technique. *Earth and Planetary Science Letters 227*, 361-376.

St-Onge, G. & Long, B. F. 2009: CAT-scan analysis of sedimentary sequences: An ultrahigh-resolution paleoclimatic tool. *Engineering Geology 103*, 127-133.

St-Onge, G., Mulder, T., Francus, P. & Long, B. 2007: Continuous Physical Properties of Cored Marine Sediments. *In* Hillaire-Marcel, C., de Vernal, A. (eds.): *Developments in Marine Geology*, *Proxies in Late Cenozoic Paleoceanography 1*, 63-98, Elsevier, Amsterdam.

St-Onge, G. & Stoner, J. 2011: Paleomagnetism Near the North Magnetic Pole: A Unique Vantage Point for Understanding the Dynamics of the Geomagnetic Field and Its Secular Variations. *Oceanography 24*, 42-50.

St-Onge, G., Stoner, J. S. & Hillaire-Marcel, C. 2003: Holocene paleomagnetic records from the St. Lawrence Estuary, eastern Canada: Centennial- to millennial-scale geomagnetic modulation of cosmogenic isotopes. *Earth and Planetary Science Letters 209*, 113-130.

Stokes, C. R., Clark, C. D., Darby, D. A. & Hodgson, D. A. 2005: Late Pleistocene ice export events into the Arctic Ocean from the M'Clure Strait Ice Stream, Canadian Arctic Archipelago. *Global and Planetary Change 49*, 139-162.

Stokes, C. R., Clark, C. D. & Winsborrow, C. M. 2006: Subglacial bedform evidence for a major palaeo-ice stream and its retreat phases in Amundsen Gulf, Canadian Arctic Archipelago. *Journal of Quaternary Science 21*, 399-412.

Stoner, J. S., Channell, J. E. T., Hillaire-Marcel, C. & Kissel, C. 2000: Geomagnetic paleointensity and environmental record from Labrador Sea core MD95-2024: Global marine sediment and ice core chronostratigraphy for the last 110 kyr. *Earth and Planetary Science Letters 183*, 161-177.

Stoner, J. S. & St-Onge, G. 2007: Magnetic Stratigraphy in Paleoceanography: Reversals, Excursions, Paleointensity, and Secular Variation. *In* Hillaire-Marcel, C., de Vernal, A. (eds.): *Developments in Marine Geology*, *Proxies in Late Cenozoic Paleoceanography 1*, 99-138, Elsevier, Amsterdam.

Stuiver, M. & Reimer, P.J. 1986-2017: CALIB 7.1 programm. http://calib.org.

Tauxe, L. 1993: Sedimentary records of relative paleointensity of the geomagnetic field: Theory and practice. *Reviews of Geophysics 31*, 319-319.

Tauxe, L., Mullender, T. A. T. & Pick, T. 1996: Potbellies, wasp-waists, and superparamagnetism in magnetic hysteresis. *Journal of Geophysical Research 101*, 571-571.

Tauxe, L., Pick, T. & Kok, Y. S. 1995: Relative paleointensity in sediments: A Pseudo-Thellier Approach. *Geophysical Research Letters 22*, 2885-2888.

Tauxe, L. & Yamazaki, T. 2007: Paleointensities. *In* Kono, M., (eds.): *Treatise on Geophysics, Geomagnetism* 5. 509-563, Elsevier, Amsterdam.

Viscosi-Shirley, C., Pisias, N. & Mammone, K. 2003: Sediment source strength, transport pathways and accumulation patterns on the Siberian-Arctic's Chukchi and Laptev shelves. *Continental Shelf Research 23*, 1201-1225.

Wagner, A., Lohmann, G. & Prange, M. 2011: Arctic river discharge trends since 7ka BP. *Global and Planetary Change 79*, 48-60.

Weingartner, T., Aagaard, K., Woodgate, R., Danielson, S., Sasaki, Y. & Cavalieri, D. 2005: Circulation on the north central Chukchi Sea shelf. *Deep Sea Research Part II: Topical Studies in Oceanography 52*, 3150-3174.

Woodgate, R. A., Aagaard, K., Swift, J. H., Falkner, K. K. & Smethie, W. M. 2005: Pacific ventilation of the Arctic Ocean's lower halocline by upwelling and diapycnal mixing over the continental margin. *Geophysical Research Letters 32*, 1-5.

Xuan, C. & Channell, J. E. T. 2010: Origin of apparent magnetic excursions in deep-sea sediments from Mendeleev-Alpha Ridge, Arctic Ocean. *Geochemistry, Geophysics, Geosystems 11*. Q02003. doi: 10.1029/2009GC002879.

Yeloff, D., Bennett, K. D., Blaauw, M., Mauquoy, D., Sillasoo, Ü., van der Plicht, J. & van Geel, B. 2006: High precision 14C dating of Holocene peat deposits: A comparison of Bayesian calibration and wiggle-matching approaches. *Quaternary Geochronology 1*, 222-235.

Zijderveld, J. D. A. 1967: A. C. Demagnetization of Rocks: Analysis of Results. *In* Collinson, D.W., Creer, K.M., Runcorn, S.K., (eds.): *Method in Paleomagnetism,* 254-286*,* Elsevier, New York.

Table captions

Table 1. Location, water depth and length of sediment cores used in this study.

Table 2. Ages from radiocarbon analyses (cores 02PC and 03PC) and cryptotephra identification (Ponomareva *et al.* 2014). Radiocarbon ages were calibrated ages using the CALIB version 7.1 software (Stuiver & Reimer 1986–2017; http://calib.org) and the Marine13 calibration curve (Reimer *et al.* 2013).

Table 3. Palaeomagnetic tie points used in this study. Tie points marked with I, D, and P correspond to inclination, declination, and palaeointensity peaks, respectively and are shown in Fig. 9. Depth in cores has been corrected for overpenetration; age is expressed as cal. a BP.

Figure captions

Fig. 1. Index map of the Beaufort and Chukchi margins and adjacent western Arctic Ocean showing location of cores 01JPC, 02PC and 03PC (red stars). Also shown is location of earlier investigated cores (grey circles) used for comparison (Polyak *et al.* 2007; Barletta *et al*. 2008, 2010; Schell *et al*. 2008; Lisé-Pronovost *et al*. 2009; Scott *et al*. 2009; Darby *et al*. 2012). The location of the Aniakchak Volcano is illustrated in the insert. ACC = Alaskan Coastal Current; BG = Beaufort Gyre.

Fig. 2. Correlation between piston and trigger weight cores (PC and TWC respectively) using k_{LF} for core 05JPC and a* for cores 02PC and 03PC. The correlation indicates that the top 110, 10, and 5 cm are missing from cores 01JPC, 02PC, and 03PC, respectively. Properties for the TWC and PC are shown in blue and red, respectively.

Fig. 3. High-resolution magnetic properties of cores 01JPC, 03PC, and 02PC. Distinct lithological facies are numbered and highlighted in grey scale. The vertical red line delineates MAD value of 5°. CT-scan images are shown for cores 03PC and 02PC. The lithology of core 01JPC is shown schematically: units Ia and Ib are characterized by homogenous light grey and olive grey sediments, respectively, and unit II consists of laminated brown to grey sediments. Arrowheads show the position of tephra (red) in core 01JPC and ^{14}C (blue) in cores 03PC and 02PC.

Fig. 4. A. Typical hysteresis curves and derived parameters. B. Day plot (Day *et al.* 1977). C. k_{ARM} *vs* k_{LF} plot representing estimated magnetic grain size for magnetite (King 1983) for cores 01JPC, 03PC and 02PC.

Fig. 5. Characteristic remanent magnetization (ChRM) and MAD values of cores 01PC, 03PC and 02PC. The red vertical line delineates MAD value of 5°. Black vertical line in the ChRM I panel represents the expected inclination for a GAD model. Grey highlighted areas indicate section breaks and intervals problematic for palaeomagnetic reconstruction.

Fig. 6. A. Comparison of the relative palaeointensity estimates based on the average ratios and the slope methods with the average ratios of NRM/ARM and NRM/IRM at 25-50 mT (core 01JPC) and 20-50 mT (cores 03PC and 02PC). B. Demagnetization curves for NRM, ARM, and IRM. C. RPI proxy *vs* its normalizer for cores 01JPC, 03PC (blue points: 100-300 cm, red points: remaining sediments), and 02PC (blue points: IRDs intervals, red points are the remaining sediments).

Fig. 7. k_{ARM}/k_{LF} ratio for cores 01JPC (this study), 06JPC, 08JPC, 05JPC from the Chukchi margin and cores 03PC (this study), 803PC, 02PC (this study) and 650PC from the Beaufort Sea. Also shown are coarse grain (>63 µm) and Fe-oxide provenance data from the Chukchi margin core P2 (Polyak *et al.* 2007). The arrows indicate a decreasing grain size trend from the last deglaciation to the Holocene.

Fig. 8. A. Age modelling using the independent ages only (^{210}Pb, ^{14}C and tephra), with palaeomagnetic tie points shown but not used in the age models. B. Composite age modelling using both the independent ages and palaeomagnetic tie points (Table 2). Age models, except for the linear model for 01JPC in Fig. 8A, are constructed using the R-package Bacon (Blaauw & Christen 2011).

Fig. 9. Full vector palaeomagnetic comparison of cores 01JPC, 03PC and 02PC with earlier developed regional records of (A) inclination, (B) declination, and (C) relative palaeointensity. Data on cores 650PC, 803PC and 05JPC are from Barletta *et al.* (2008, 2010), core 16JPC from Darby *et al.* (2012), and cores 06JPC and 08JPC from Lisé-Pronovost *et al.* (2009). Also shown are the CALS10k spherical harmonic model outputs for the Beaufort margin (71.61° N, 137.54° W; derived from Korte *et al.* 2011).

Fig. 10. Age model for cores from the Beaufort Sea. Cores 124PC and 750PC are from Scott *et al*. (2009), cores 650PC and 803PC from Barletta *et al.* (2008, 2010), and cores PC1, PC2 and PC3 from Schell *et al*. (2008). Also shown is reconstruction of the relative sea level from Hill *et al*. (1993) and Héquette *et al*. (1995). SRSL = slow rising sea level; HSRL = high rising sea level; MW = meltwater.

Supporting information

Fig. S1. Magnetic susceptibility comparison of cores 2004-804-750PC (Scott *et al.* 2009) and 02PC. Yellow circles represent depths of radiocarbon dating (Scott *et al.* 2009).

Fig. S2. Core-top correlation using the optical properties (L*, a* and b*) between the 01MC and 01TWC. The results indicates there is no correlation between 01MC and 01TWC and suggesting that the first 45 cm are missing at the top of the TWC.

Fig. S3. 210Pb and carbon content measurements for box core HLY01-01MC. A. ^{210}Pb total activity (dpm: disintegration per minute) in the top 15 cm. The supported ^{210}Pb activity is illustrated by the vertical black line. B. Napierian logarithm of the210Pb excess activity used for the estimation of the sedimentation rate. C. Total (red) and organic (blue) carbon contents.

Fig. S4. Orthogonal projection diagrams (Zijderveld 1967) at three selected depths for cores 01JPC, 03PC, and 02PC. Open (closed) symbols represent vector end points projected on the vertical (horizontal) plane, respectively.

Fig. S5. Box-plot of several magnetic properties of marine cores on the North American margin along a west-east transect for the Holocene (red) and the deglaciation (blue). The mean values for both areas and periods are given by the horizontal lines. The box plots showed the median (horizontal line) and the box includes 50% of the distribution. Data from cores 06JPCand 08JPC are from Lisé-Pronovost *et al*. (2009) and cores 05JPC, 650PC, and 803PC are from Barletta *et al.* (2008, 2010).

Figure S6. Ratio Fe/kLF for cores 01JPC, 03PC and 02PC indicative reductive diagenesis when Fe/kLF >40 Mcps (Funk *et al*. 2004; Hofmann *et al*. 2005).

Fig. S7. Diffractogram of the cores 01JPC, 03PC and 02PC with the addition 0.111 g of zincite to 1 g of bulk sediment following the protocole of Eberl (2003). Briefly, 0.111 g of zincite was added to 1 g of bulk sediment. Samples were X-rayed from 5 to 65 degrees two theta with Cu K-alpha radiation (45 kV, 40 mA) using a PANalytical X'Pert Powder diffractometer. The XRD data were converted into weight percent minerals using the RockJock computer program (Eberl 2003; Ortiz *et al*. 2009; Andrews & Eberl 2012; Andrews *et al*. 2013).

Table S1: Number of ^{14}C datation, chronostratigraphic tie points and if model comparison were applied on the core 16JPC, 05JPC, 06JPC, 08JPC, 803PC and 650PC used in this study for comparison (Barletta *et al*. 2008, 2010; Lisé-Pronovost *et al.* 2009; Darby *et al.* 2012).

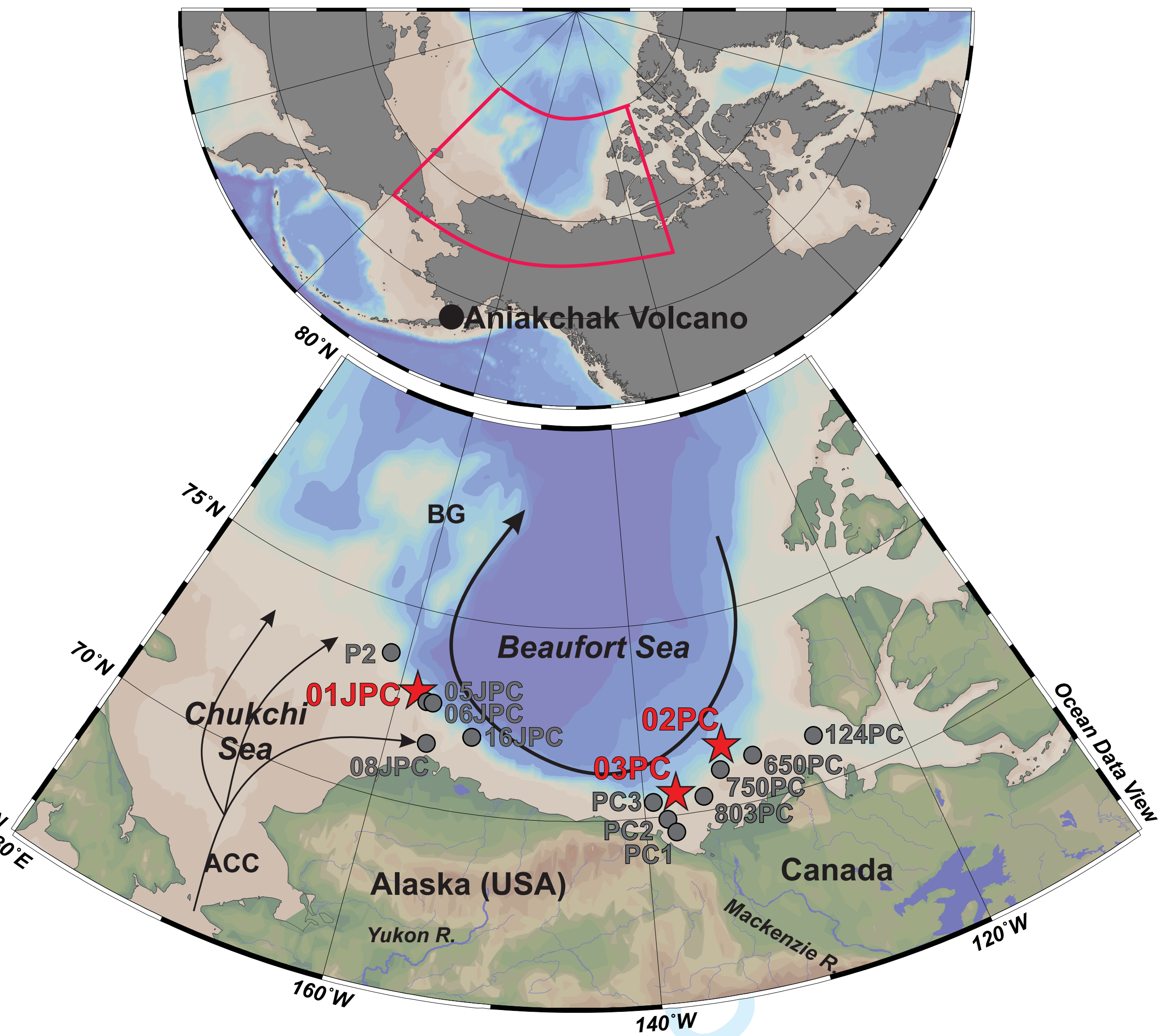
Aniakchak Volcano
80°N
75°N
70°N
65°N
180°E
160°W
140°W
120°W
BG
Beaufort Sea
Chukchi Sea
ACC
P2
01JPC
05JPC
06JPC
16JPC
08JPC
02PC
03PC
124PC
650PC
750PC
803PC
PC3
PC2
PC1
Alaska (USA)
Canada
Yukon R.
Mackenzie R.
Ocean Data View

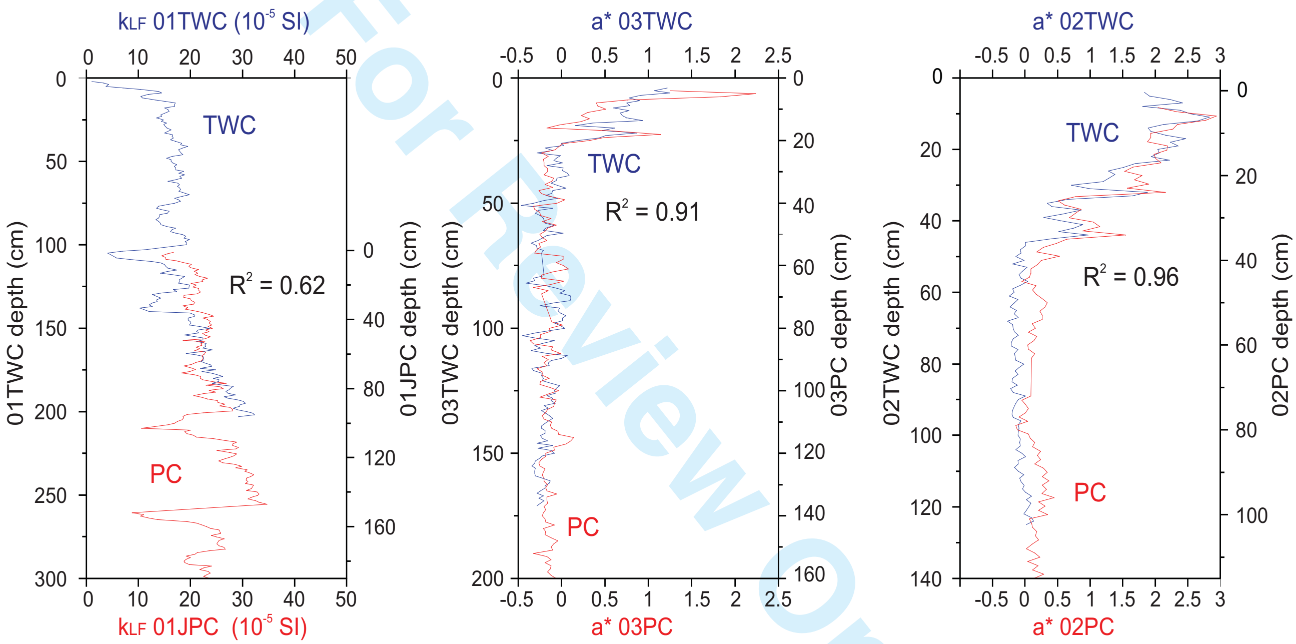
kLF 01TWC (10-5 SI)
TWC
PC
R2 = 0.62
01TWC depth (cm)
01JPC depth (cm)
kLF 01JPC (10-5 SI)
a* 03TWC
TWC
R2 = 0.91
PC
03TWC depth (cm)
03PC depth (cm)
a* 03PC
a* 02TWC
TWC
R2 = 0.96
PC
02TWC depth (cm)
02PC depth (cm)
a* 02PC
For Review Only

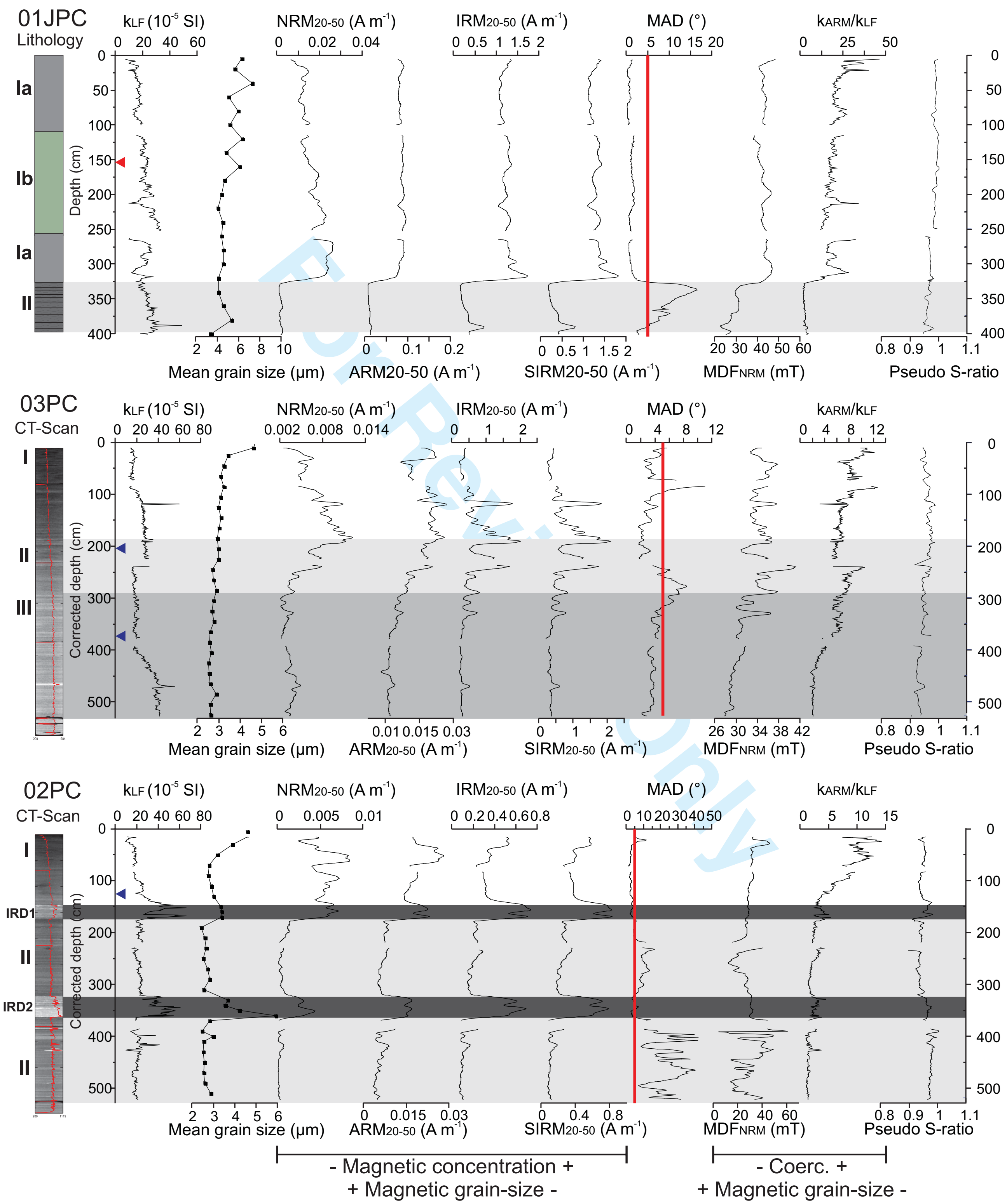
01JPC
Lithology
Ia
Ib
Ia
II
kLF (10-5 SI)
NRM20-50 (A m-1)
IRM20-50 (A m-1)
MAD (°)
kARM/kLF
Depth (cm)
Mean grain size (µm)
ARM20-50 (A m-1)
SIRM20-50 (A m-1)
MDFNRM (mT)
Pseudo S-ratio
03PC
CT-Scan
I
II
III
Corrected depth (cm)
02PC
CT-Scan
I
IRD1
II
IRD2
II
- Magnetic concentration +
+ Magnetic grain-size -
- Coerc. +
+ Magnetic grain-size -

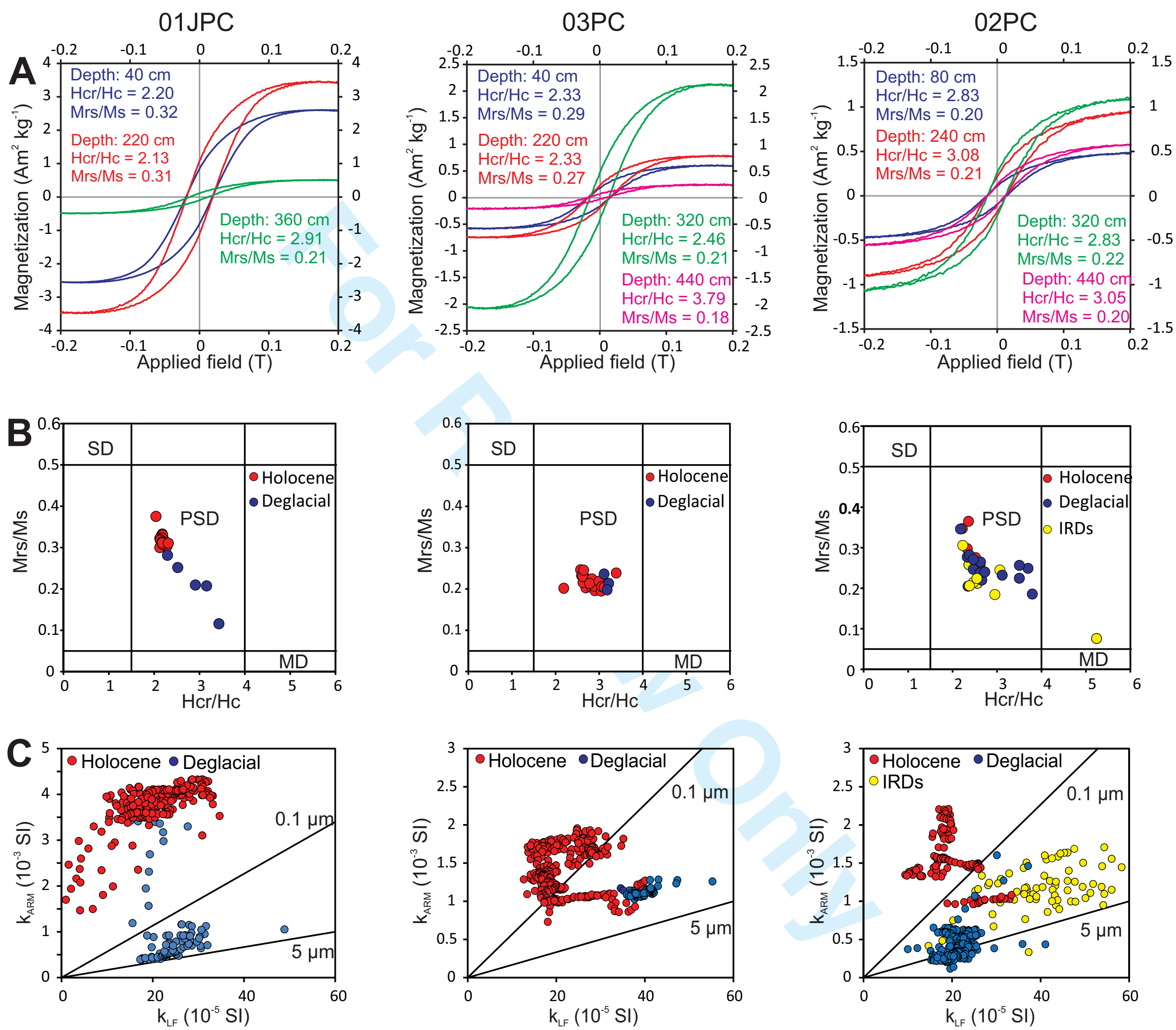
01JPC
03PC
02PC
A
B
C
Depth: 40 cm
Hcr/Hc = 2.20
Mrs/Ms = 0.32
Depth: 220 cm
Hcr/Hc = 2.13
Mrs/Ms = 0.31
Depth: 360 cm
Hcr/Hc = 2.91
Mrs/Ms = 0.21
Depth: 40 cm
Hcr/Hc = 2.33
Mrs/Ms = 0.29
Depth: 220 cm
Hcr/Hc = 2.33
Mrs/Ms = 0.27
Depth: 320 cm
Hcr/Hc = 2.46
Mrs/Ms = 0.21
Depth: 440 cm
Hcr/Hc = 3.79
Mrs/Ms = 0.18
Depth: 80 cm
Hcr/Hc = 2.83
Mrs/Ms = 0.20
Depth: 240 cm
Hcr/Hc = 3.08
Mrs/Ms = 0.21
Depth: 320 cm
Hcr/Hc = 2.83
Mrs/Ms = 0.22
Depth: 440 cm
Hcr/Hc = 3.05
Mrs/Ms = 0.20
Magnetization (Am² kg⁻¹)
Applied field (T)
SD
PSD
MD
Holocene
Deglacial
IRDs
Mrs/Ms
Hcr/Hc
0.1 µm
5 µm
k_ARM (10⁻³ SI)
k_LF (10⁻⁵ SI)

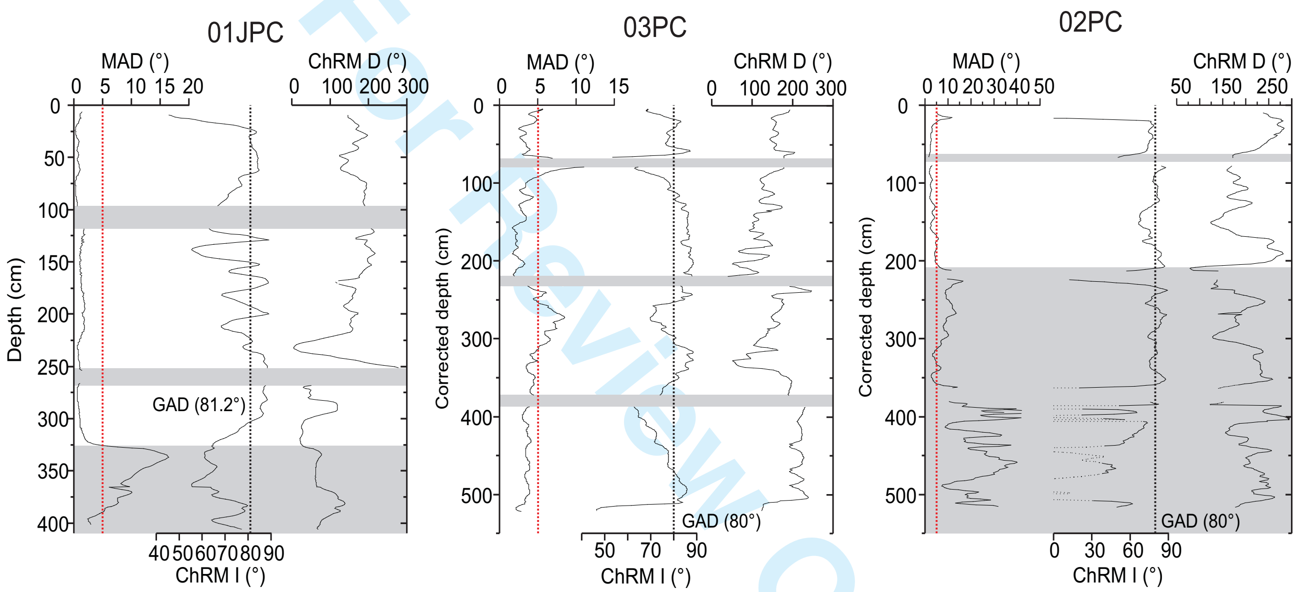
01JPC
MAD (°)
ChRM D (°)
Depth (cm)
GAD (81.2°)
ChRM I (°)
03PC
Corrected depth (cm)
GAD (80°)
02PC

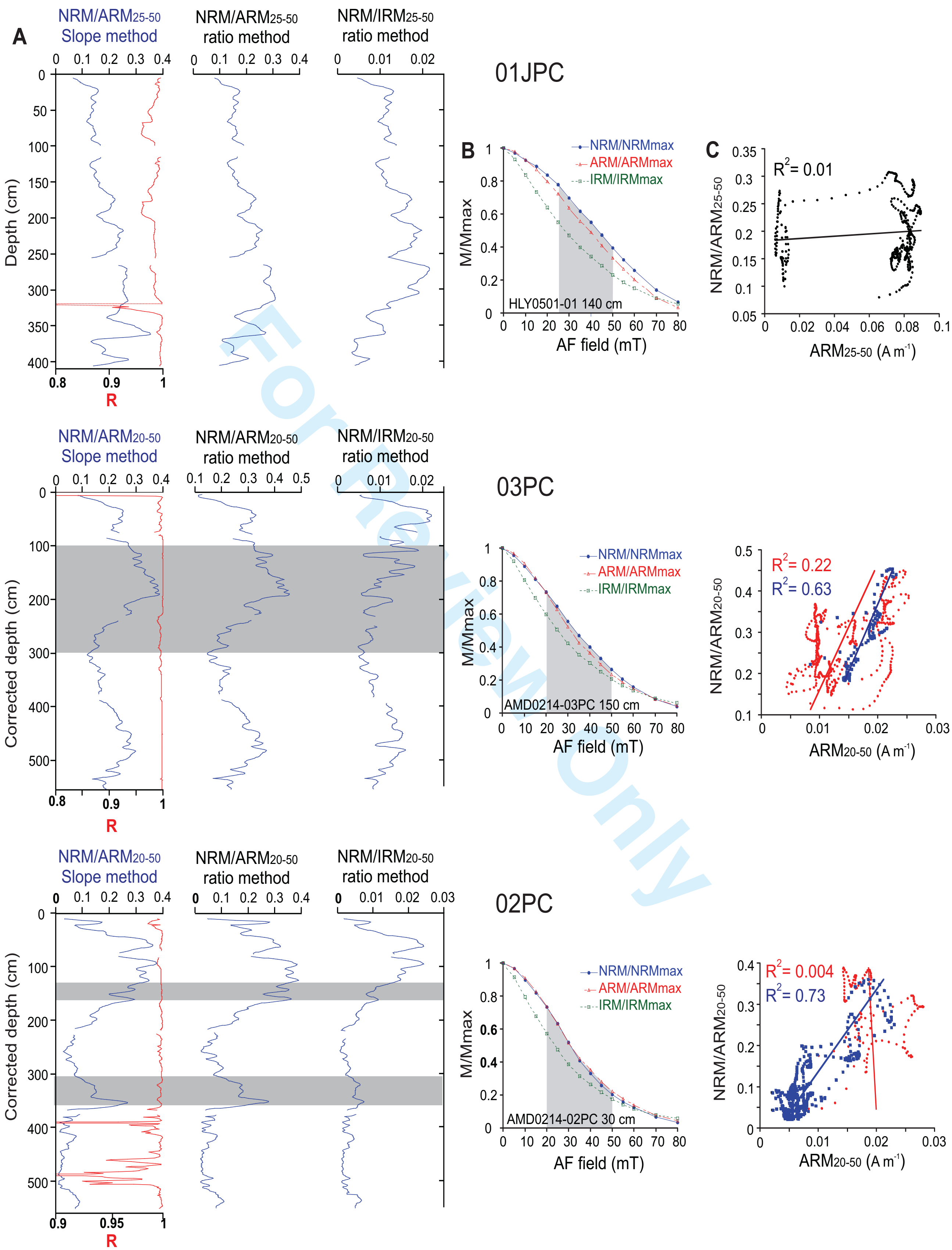
A
NRM/ARM25-50
Slope method
NRM/ARM25-50
ratio method
NRM/IRM25-50
ratio method
01JPC
Depth (cm)
R
B
NRM/NRMmax
ARM/ARMmax
IRM/IRMmax
M/Mmax
HLY0501-01 140 cm
AF field (mT)
C
R^2= 0.01
NRM/ARM25-50
ARM25-50 (A m-1)
NRM/ARM20-50
Slope method
NRM/ARM20-50
ratio method
NRM/IRM20-50
ratio method
03PC
Corrected depth (cm)
R
NRM/NRMmax
ARM/ARMmax
IRM/IRMmax
M/Mmax
AMD0214-03PC 150 cm
AF field (mT)
R^2= 0.22
R^2= 0.63
NRM/ARM20-50
ARM20-50 (A m-1)
NRM/ARM20-50
Slope method
NRM/ARM20-50
ratio method
NRM/IRM20-50
ratio method
02PC
Corrected depth (cm)
R
NRM/NRMmax
ARM/ARMmax
IRM/IRMmax
M/Mmax
AMD0214-02PC 30 cm
AF field (mT)
R^2= 0.004
R^2= 0.73
NRM/ARM20-50
ARM20-50 (A m-1)

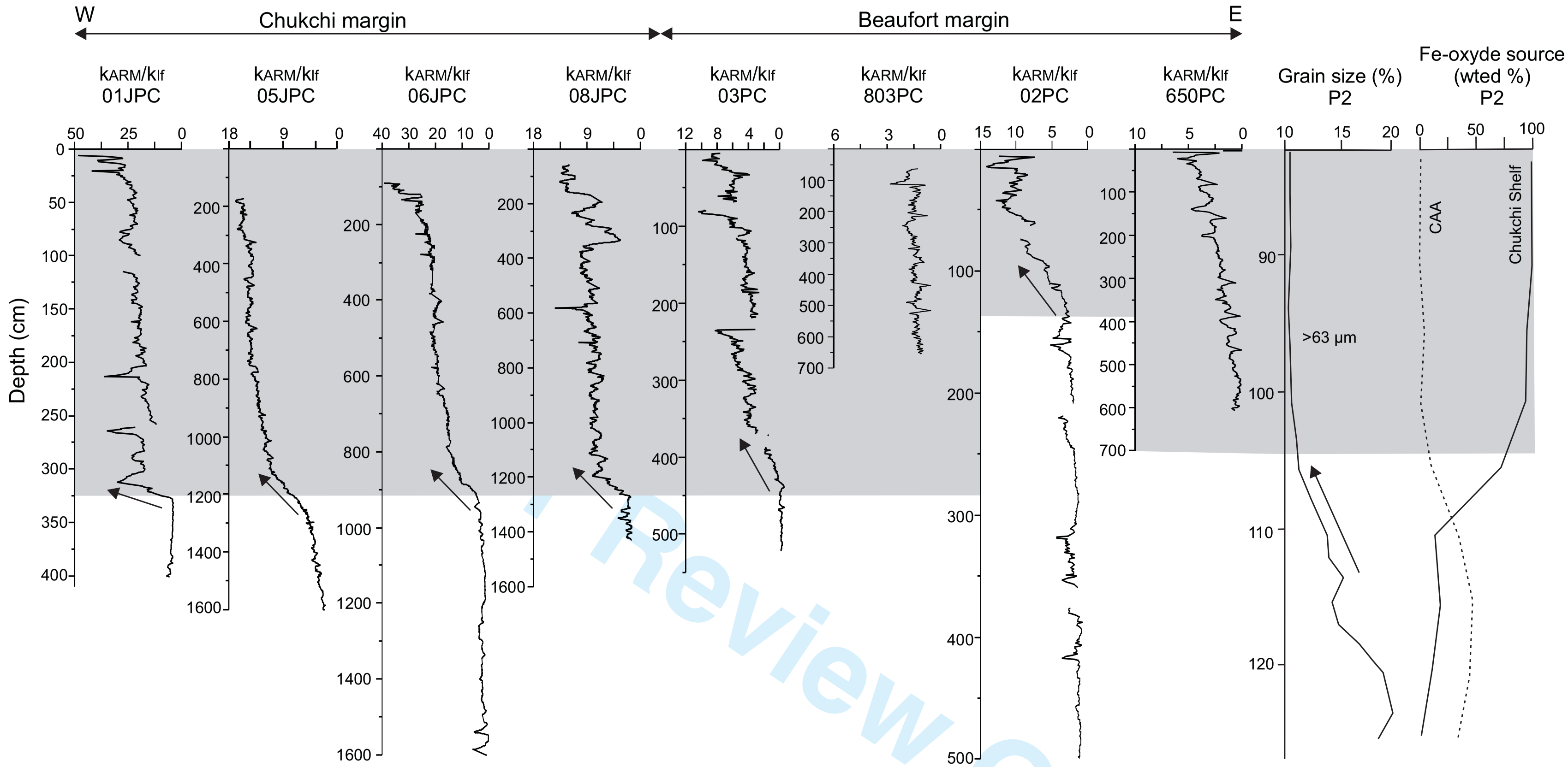
W
Chukchi margin
Beaufort margin
E
kARM/klf
01JPC
05JPC
06JPC
08JPC
03PC
803PC
02PC
650PC
Grain size (%)
P2
Fe-oxyde source
(wted %)
P2
Depth (cm)
>63 µm
CAA
Chukchi Shelf

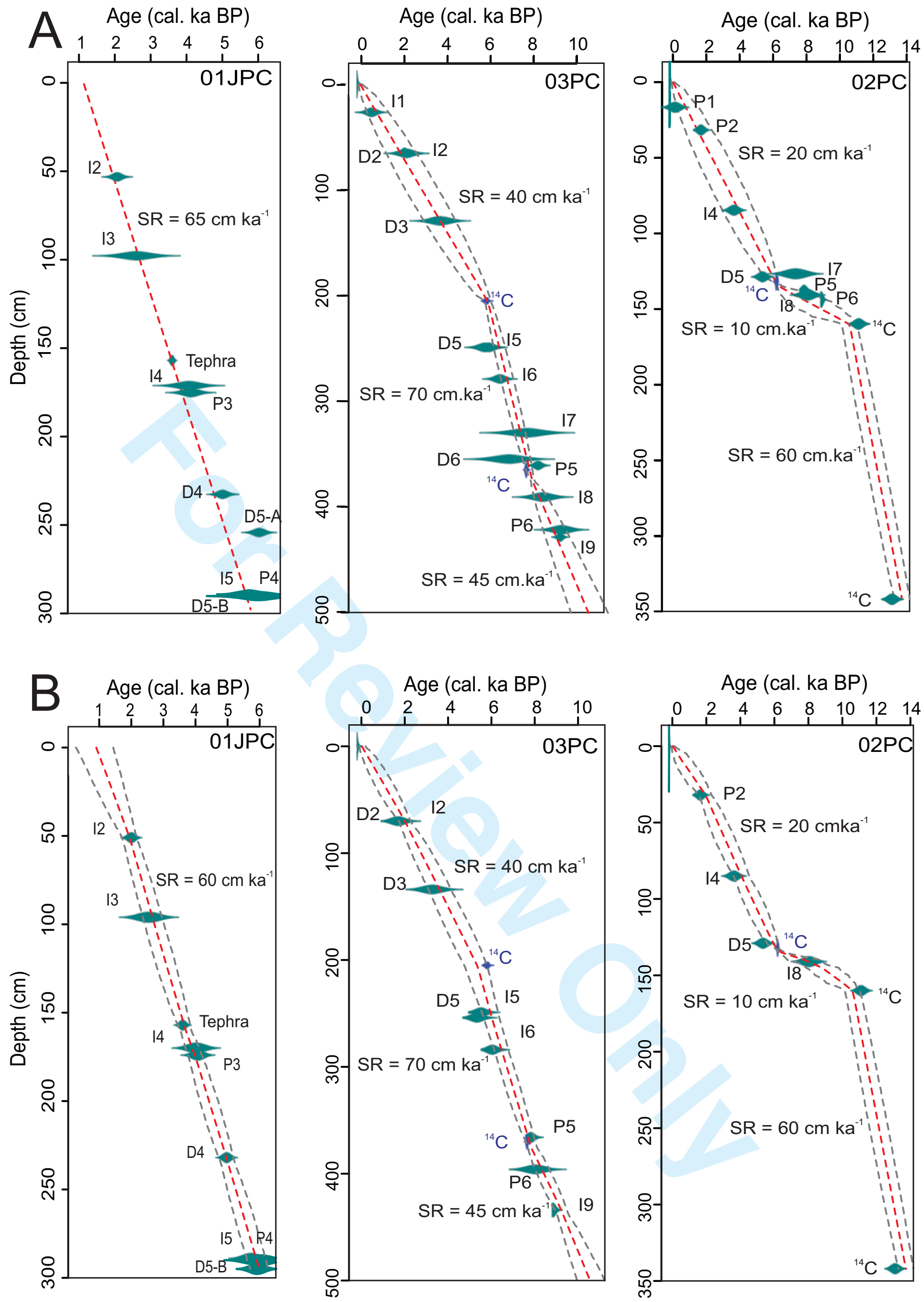
A
B
Age (cal. ka BP)
Depth (cm)
01JPC
03PC
02PC
SR = 65 cm ka-1
SR = 40 cm ka-1
SR = 70 cm.ka-1
SR = 45 cm.ka-1
SR = 20 cm ka-1
SR = 10 cm.ka-1
SR = 60 cm.ka-1
SR = 60 cm ka-1
SR = 40 cm ka-1
SR = 70 cm ka-1
SR = 45 cm ka-1
SR = 20 cmka-1
SR = 10 cm ka-1
SR = 60 cm ka-1
Tephra
I1
I2
I3
I4
I5
I6
I7
I8
I9
D2
D3
D4
D5
D5-A
D5-B
D6
P1
P2
P3
P4
P5
P6
14C

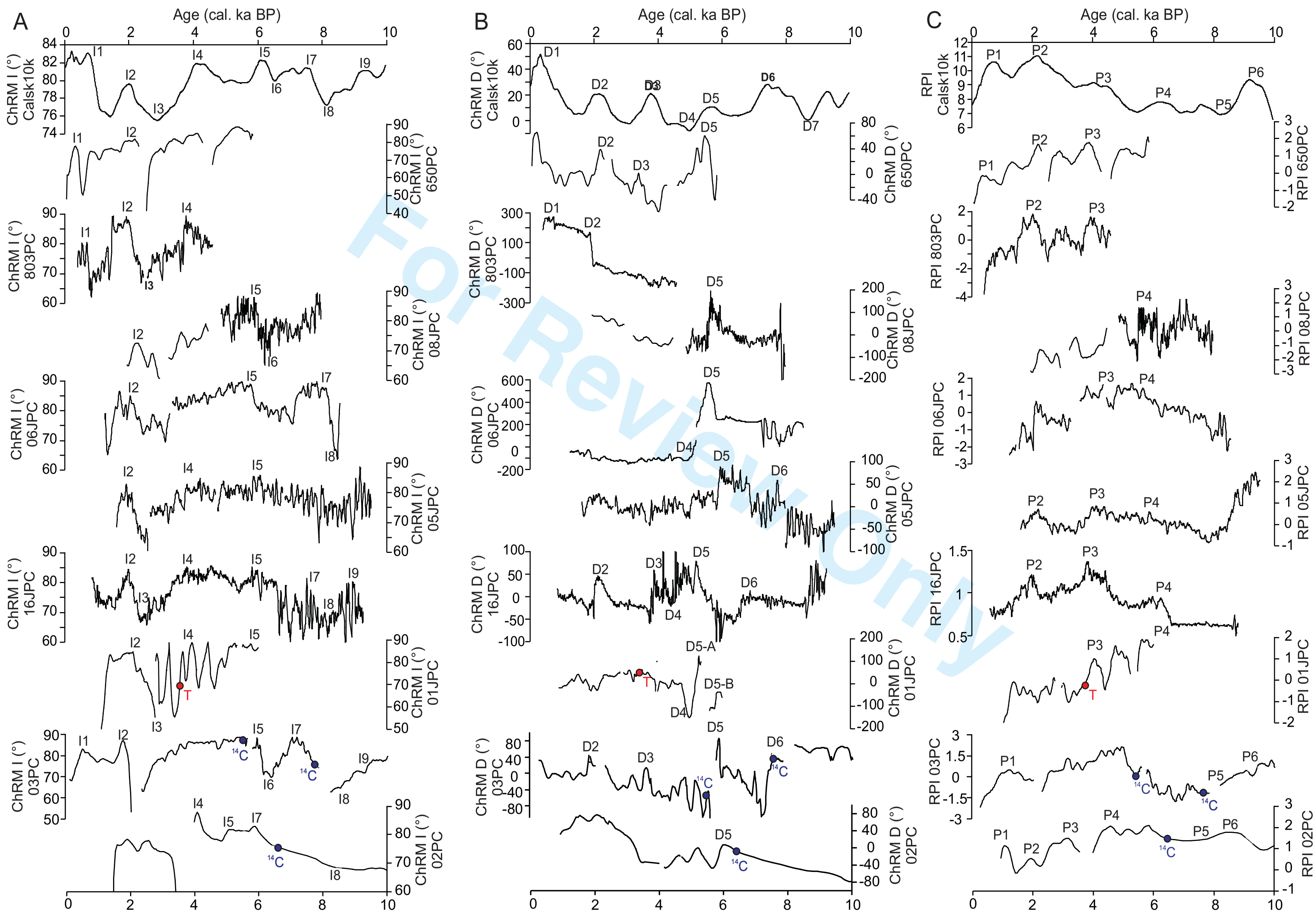
A
B
C
Age (cal. ka BP)
ChRM I (°) Calsk10k
ChRM I (°) 650PC
ChRM I (°) 803PC
ChRM I (°) 08JPC
ChRM I (°) 06JPC
ChRM I (°) 05JPC
ChRM I (°) 16JPC
ChRM I (°) 01JPC
ChRM I (°) 03PC
ChRM I (°) 02PC
ChRM D (°) Calsk10k
ChRM D (°) 650PC
ChRM D (°) 803PC
ChRM D (°) 08JPC
ChRM D (°) 06JPC
ChRM D (°) 05JPC
ChRM D (°) 16JPC
ChRM D (°) 01JPC
ChRM D (°) 03PC
ChRM D (°) 02PC
RPI Calsk10k
RPI 650PC
RPI 803PC
RPI 08JPC
RPI 06JPC
RPI 05JPC
RPI 16JPC
RPI 01JPC
RPI 03PC
RPI 02PC
I1 I2 I3 I4 I5 I6 I7 I8 I9
D1 D2 D3 D4 D5 D5-A D5-B D6 D7
P1 P2 P3 P4 P5 P6
T
^{14}C

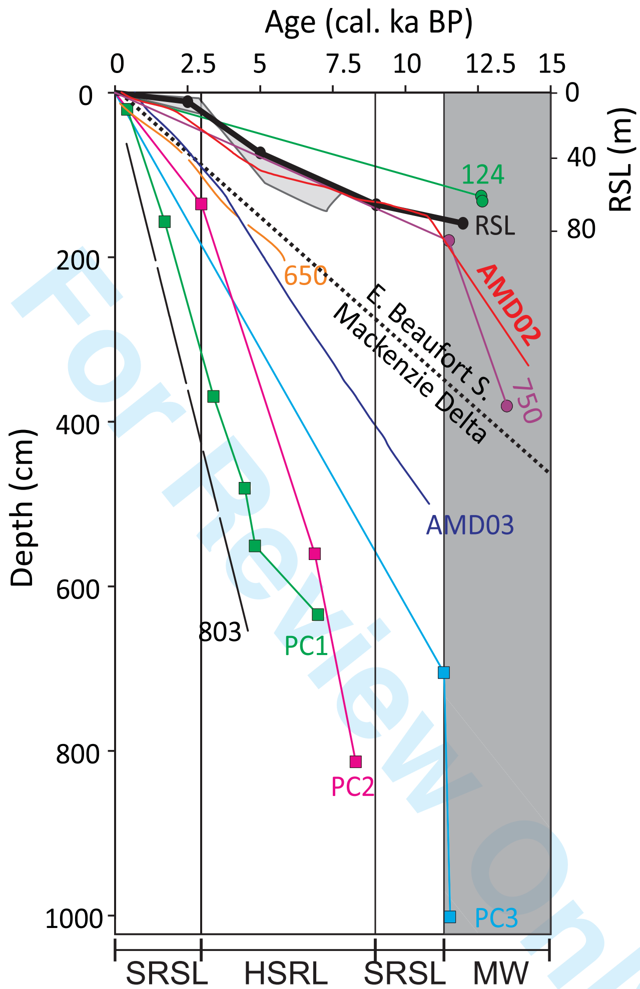
Age (cal. ka BP)
0
2.5
5
7.5
10
12.5
15
RSL (m)
0
40
80
Depth (cm)
0
200
400
600
800
1000
124
RSL
AMD02
750
650
E. Beaufort S.
Mackenzie Delta
AMD03
803
PC1
PC2
PC3
SRSL
HSRL
SRSL
MW

Core	Latitude (DD)	Longitude (DD)	Water depth (m)	Length (m)
01JPC/TWC	72.90	-158.42	1163	13.72/2
01MC	72.90	-158.42	unknown	0.5
02PC/TWC	71.61	-133.57	998	5.48/1.32
03PC/TWC	70.55	-137.54	1051	5.85/1.74

Core	Depth (cm)	Corrected depth (cm)	Material	Conventionnal age	Calibrated age (cal. a BP)	Lab. number
01JPC	157	-	Cryptotephra	-	3600	-
03PC	200	205	Foraminifers (mixed)	5831±70	5631 (5800) 5946	ECHo1870
03PC	365	370	Foraminifers (mixed)	7590±30	7755 (7645) 7555	Beta-429147
02PC	122	132	Foraminifers (mixed)	6160±30	6395 (6520) 6655	Beta-430871

Tie point	Depth 03PC	Depth 02PC	Depth 01JPC	Age Cals10k	Age 650PC	Age 803PC	Age 05JPC	Age 06JPC	Age 08JPC	Age 16JPC	Mean age	SD age (1σ)
I1	31	-	-	600	340	445	-	-	-	-	462	107
I2	69	-	51	2010	2110	1920	1920	2068.4	2010	1975.5	2002	66
I3	-	-	96	2885	-	2450	2585	2490	2570	2313	2548	175
I4	-	85	170	4010	-	4140	4145	-	-	3793	4022	143
I5	254	-	295	6100	-	-	6040	5830	5815	5823	5921	122
I6	284	-	-	6525	-	-	-	6520	6280	-	6442	114
I7	335	127	-	7460	-	-	-	8155	-	7524	7713	313
I8	397	141	-	8630	-	-	-	8515	-	8159	8434	200
I9	427	-	-	9310	-	-	-	-	-	8952	9131	179
D1	-	-	-	225	200	-	-	-	-	-	212.5	12.5
D2	70	-	-	2240	2200	1865	-	-	-	2074.5	2095	146
D3	135	-	-	3730	3390	-	-	-	-	3870	3663	201
D4	-	99	232	4990	-	-	-	4900	4930	5068	4972	64
D5A	254	129	255	5700	-	-	5954	5630	5640	5193	5731	131.50
D5B			289									
D6	360	-	-	7430	-	-	7580	-	-	6871	7293	305
P1	46	17	-	660	340	-	-	-	-	-	500	160
P2	-	32	-	2160	2180	2015	1940	-	-	1939.5	2047	105
P3	-	-	174	4050	4000	4035	4025	4050	-	4300	4076	101
P4	-	-	290	6250	-	-	5855	5685	5950	6174.5	5982	207
P5	366	138	-	8300	-	-	8130	-	-	-	8215	85
P6	434	144	-	9190	-	-	9300	-	-	-	9245	55

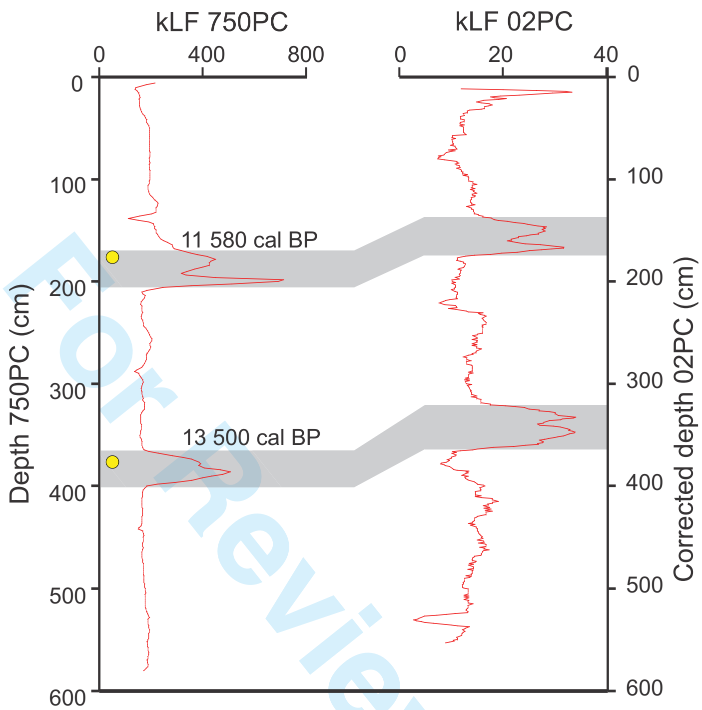

Figure S1: Magnetic susceptibility comparison of cores 2004-804-750PC (Scott *et al.* 2009) and 02PC. Yellow circles represent depths of radiocarbon dating (Scott *et al.* 2009).

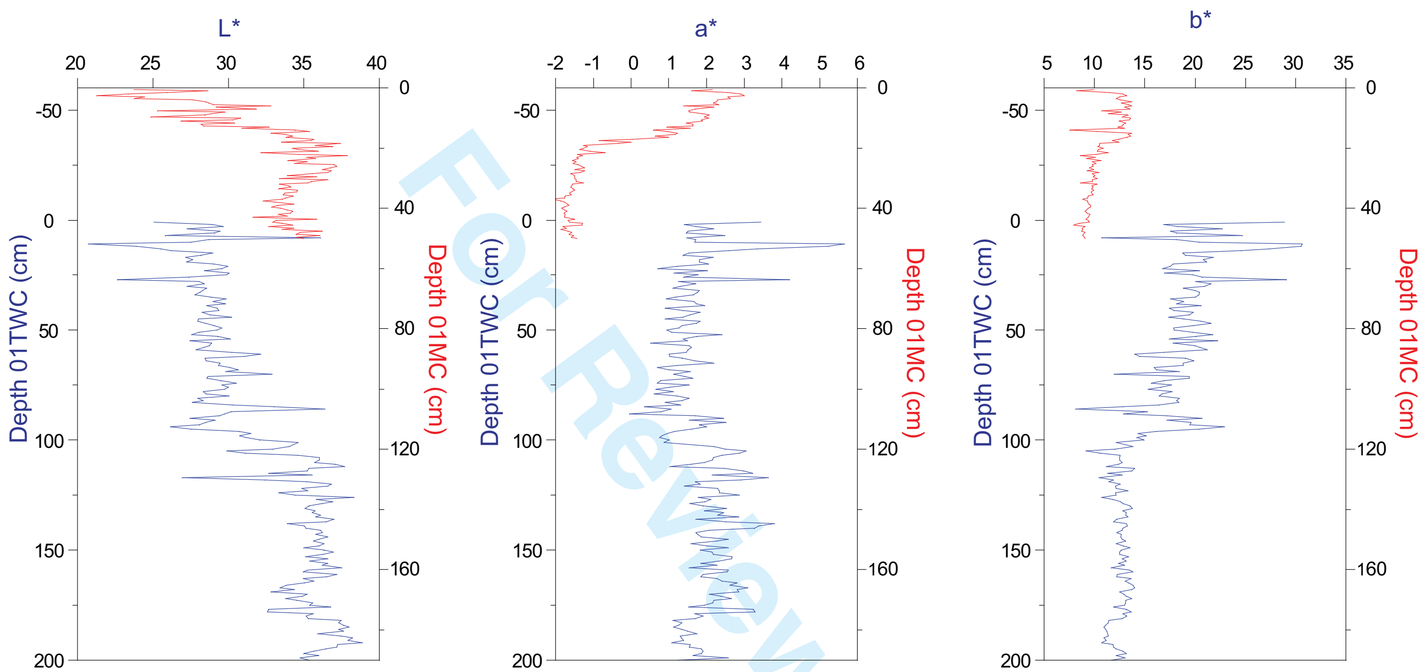

Fig. S2. Core-top correlation using the optical properties (L*, a* and b*) between the 01MC and 01TWC. The results indicates there is no correlation between 01MC and 01TWC and suggesting that the first 45 cm are missing at the top of the TWC.

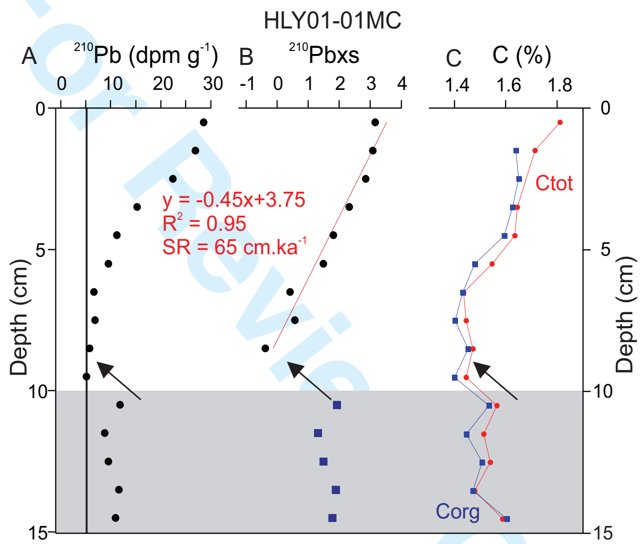

Figure S3. ^{210}Pb and carbon content measurements for box core HLY01-01MC. A. ^{210}Pb total activity (dpm: disintegration per minute) in the top 15 cm. The supported ^{210}Pb activity is illustrated by the vertical black line. B. Napierian logarithm of the ^{210}Pb excess activity used for the estimation of the sedimentation rate. C. Total (red) and organic (blue) carbon contents.

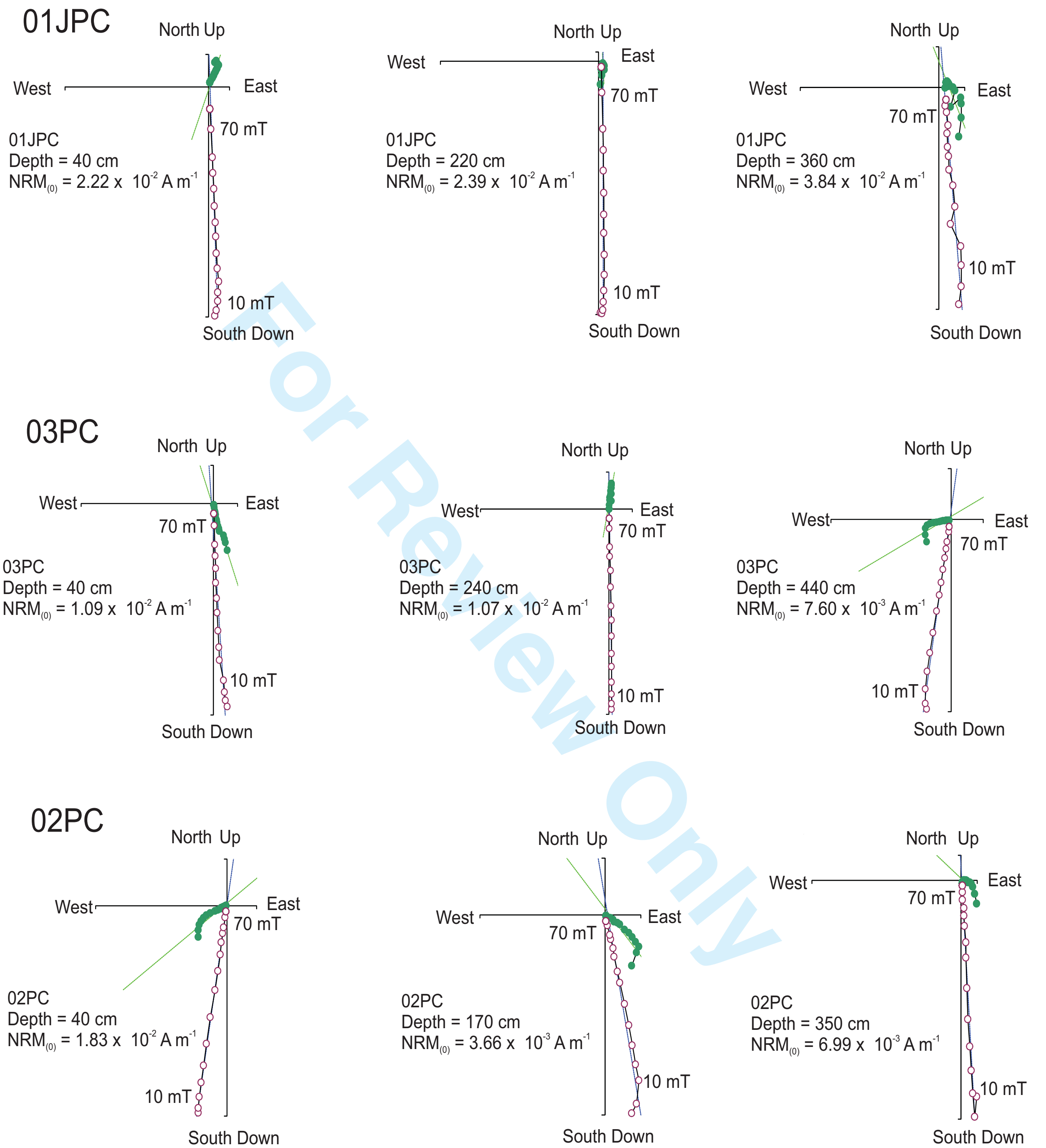

Figure S4. Orthogonal projection diagrams (Zijderveld 1967) at three selected depths for cores 01JPC, 03PC, and 02PC. Open (closed) symbols represent vector end points projected on the vertical (horizontal) plane, respectively.

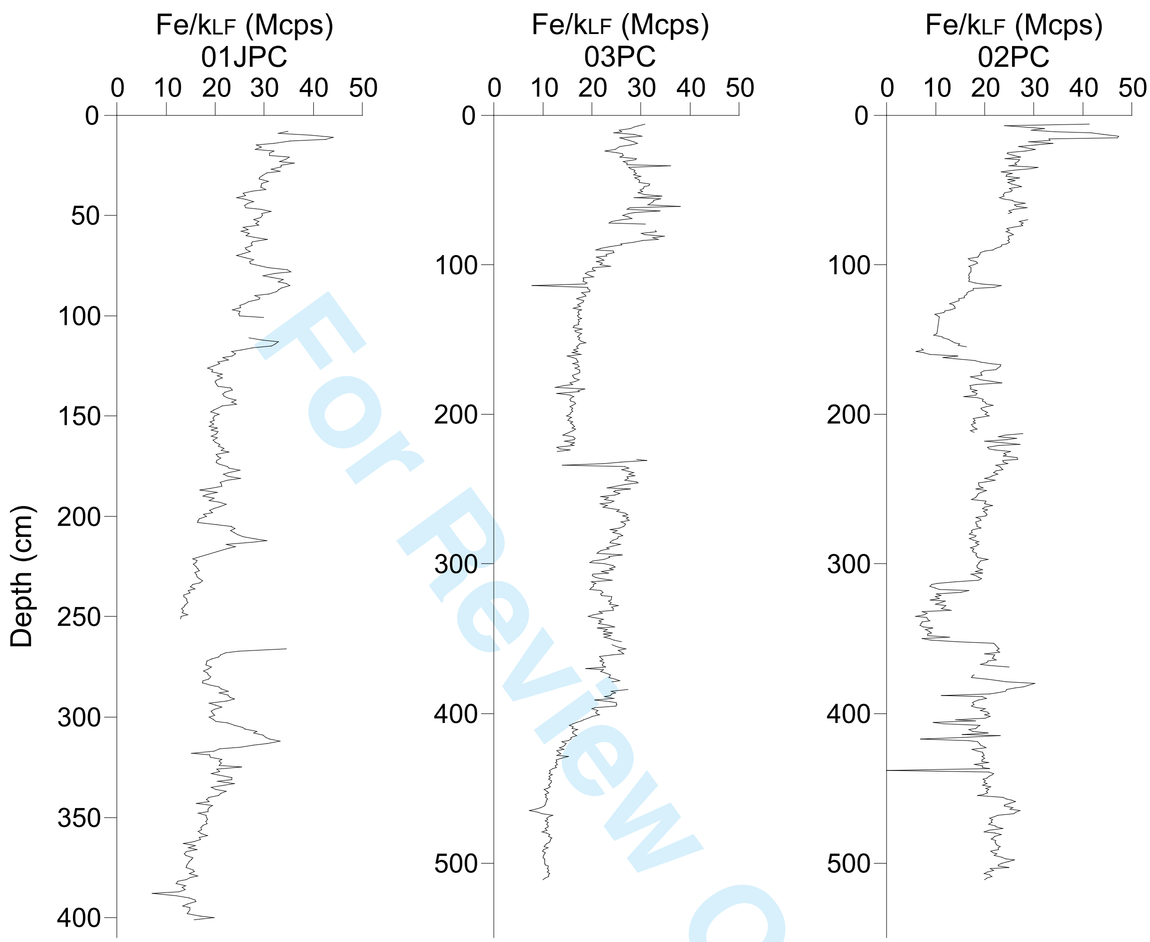

Figure S6. Ratio Fe/kLF for cores 01JPC, 03PC and 02PC indicative reductive diagenesis when Fe/kLF >40 Mcps (Funk *et al.* 2004; Hofmann *et al.* 2005).

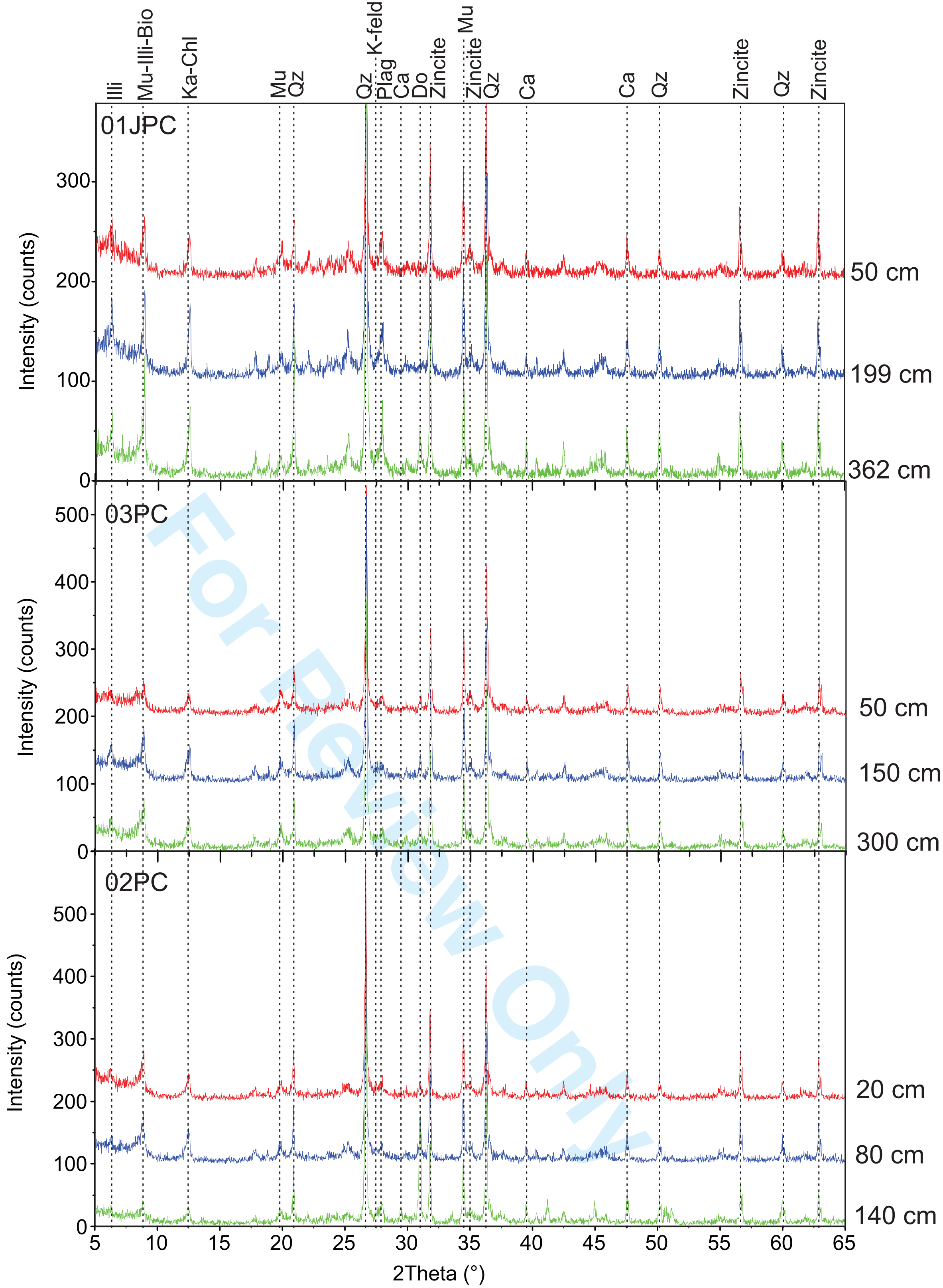

Figure S7. Diffractogram of the cores 01JPC, 03PC and 02PC with the addition 0.111 g of zincite to 1 g of bulk sediment following the protocole of Eberl (2003). Briefly, 0.111 g of zincite was added to 1 g of bulk sediment. Samples were X-rayed from 5 to 65 degrees two theta with Cu K-alpha radiation (45 kV, 40 mA) using a PANalytical X'Pert Powder diffractometer. The XRD data were converted into weight percent minerals using the RockJock computer program (Eberl 2003; Ortiz *et al*. 2009; Andrews & Eberl 2012; Andrews *et al*. 2013).

Table S1: Number of ^{14}C datation, chronostratigraphic tie points and if model comparison were applied on the core 16JPC, 05JPC, 06JPC, 08JPC, 803PC and 650PC used in this study for comparison (Barletta *et al*. 2008, 2010; Lisé-Pronovost *et al.* 2009; Darby *et al.* 2012).

Cores	Nb. ^{14}C	Nb. tie points	Model comparison
16JPC	4	39	yes
05JPC	6	6	yes
06JPC	1	10	yes
08JPC	9	10	yes
803PC	4	6	yes
650PC	1	17	yes